The role of the neuronal gap junction protein connexin36 in kainic acid induced hippocampal excitotoxicity

Mark S Akins

A thesis submitted to the Faculty of Graduate and Postdoctoral studies in partial fulfillment of the requirements for the degree of Masters of Science.

Department of Biochemistry, Microbiology and Immunology
University of Ottawa
Ottawa, ON, Canada

Abstract

Kainic acid induced excitotoxicity causes pyramidal cell death in the CA3a/b region of the hippocampus. Electrical synapses, gap junctional communication, and single membrane channels in non-junctional membranes (hemichannels) composed of connexin36 (Cx36) have been implicated in both seizure propagation and the spread of excitotoxic cell death. In rats, Cx36 protein is expressed by pyramidal neurons. Localization of protein in mouse, however, is highly controversial. Expression is reported to be restricted to hippocampal interneurons yet the same excitotoxic mechanisms (electrical and metabolic coupling between pyramidal neurons) are invoked to explain the role of Cx36 in excitotoxic pyramidal loss in murine brain. To address this controversy, I show by confocal immunofluorescence and *in situ* hybridization that Cx36 protein expression is restricted to interneurons and microglia in murine hippocampus and is not expressed by, or is below level of detection in pyramidal neurons. Using behavioural and electrophysiological measures, seizure propagation was found to be moderately enhanced in the absence of Cx36 likely due to the loss of interneuron-mediated synchronous inhibition of the pyramidal cells. Further, CA3a/b neurons die post kainic acid injury in the presence of Cx36 but are protected in $Cx36^{-/-}$ mice. When delayed excitotoxic cell death is maximal, Cx36 is primarily expressed by activated microglia as demonstrated by confocal immunofluorescence, *in situ* hybridization, and Western blotting. These activated microglia are located in the direct vicinity of, and surrounding cells in the damaged Ca3a/b region. Finally, I show that loss of Cx36 from activated microglia in mice is sufficient to prevent excitotoxic cell death in the

CA3a/b with surviving neurons functional as assessed by both electrophysiological and behavioural measures. Together, these data identify a new mechanism of excitotoxic injury, mediated by neuronal-glial interactions, and dependent on microglial Cx36 expression.

Acknowledgements

I would like to give sincere thanks to my supervisor, Dr. Steffany Ann Larwill Bennett for her excellent advice, guidance, and assistance throughout the duration of my Master's and for her continued support. Without her insight this thesis surely would not have reached the level it achieved. I would also like to thank Bennett lab members, of past and present for their help, guidance, assistance and for standing by me. I would like to specifically thank Catherine Sorbara for her outstanding scientific skill, help with the project, and most of all for great friendship that will last a lifetime. Along the same lines, I would like to thank Dr. Leigh-Anne Swayne for her out-of-sight insight and knowledge base, her advice on scientific matters was priceless, Leigh-Anne became a great friend, one that I am truly thankful to have. I would also like to thank Dr. Leo Renaud, and Dr. David Spanswick for their guidance and assistance in the electrophysiology experiments. I would also like to thank my thesis advisory committee Dr. Ilona Skeranj, and Dr. Diane Lagace for their guidance, insight and support over the duration of my Master's project. Finally, I would like to thank my family: My wife Joanne, and my two beautiful, inspirational girls, Sadie and Heather; you both are truly my little heroes.

Table of Contents

List of Abbreviations

4-AP	4-aminopyridine
aCSF	Artificial cerebrospinal fluid
AD	Alzheimer disease
AED	Anti epileptic drugs
AMPA	L-α-amino-3-hydroxy-5-methylisoxazole-4-propionate
AMPAR	L-α-amino-3-hydroxy-5-methylisoxazole-4-propionate receptor
ATP	Adenosine triphosphate
BBB	Blood brain barrier
BR	Back right
BrdU	5-bromo-2-deoxyuridine
CldU	5-chloro-2-deoxyuridine
Ca(1-3)	Cornu ammonis (1-3)
cAMP	Cyclic adenosine monophosphate
Cx	Connexin
DG	Dentate gyrus
DIG	Digoxigenin
DNA	Deoxyribonucleic acid
D-AP5	D-(-)-2-Amino-5-phosphonopentanoic acid
EPSP	Excitatory post synaptic potential
FL	Front left
GABA	Gamma aminobutyric acid
GJ	Gap junction
GJIC	Gap junctional intercellular communication
H&E	Haematoxylin & eosin
HC	Hemichannel
Iba1	Ionized calcium adaptor molecule 1
IPSP	Inhibitory post synaptic potential
IdU	5-iodo-2-deoxyuridine
KA	Kainic acid
KO	Knock out
kDa	Kilodaltons
mRNA	Messenger ribonucleic acid
MWM	Morris water maze
NBQX	6-nitro-7-sulphamoylbenzo(f)-quinoxaline-2,3-dione
NMDA	N-methyl-D-aspartate
NMDAR	N-methyl-D-aspartate receptor
NO	Nitric oxide
PARV	Parvalbumin
PD	Parkinson's disease
PLAP	Placental alkaline phosphatase
PBS	Phosphate buffered saline
ROS	Reactive oxygen species
Slu	Stratum lucidum
SGZ	Sub granular zone

So	Stratum oriens
Sr	Stratum radiatum
SVZ	Sub ventricular zone
TLE	Temporal lobe epilepsy
TUNEL	Terminal deoxynucleotidyl transferase dUTP nick end labeling

List of Figures

List of Tables

1. Chapter 1 – General introduction

1.1 The connexin family of gap junction proteins.

Connexins (Cx) are a family of proteins that facilitate cellular communication in eukaryotic organisms. Connexins are composed of four transmembrane spanning proteins with two extracellular loops, an intracellular loop, and intracellular carboxy and amino termini (Fig. 1.1a)[1; 2]. When six connexins hexamerize they form a connexon (Figure 1b,c). When integrated into the plasma membrane, a connexon is a pore-like structure allowing for the passage of small molecules <1.2 kiloDaltons (kDa) such as ions, second messengers and metabolites including Na^+, K^+, Ca^{2+}, inositol-1,4,5-trisphosphate, and cyclic AMP[3; 4]. In non-junctional membranes, these hemichannels (or single membrane channels) enable cellular communication with the extracellular space (Fig. 1.1d)[5; 6]. When connexons of adjacent cells dock with one another they can form a functional intercellular channel, facilitating gap junctional intercellular communication (GJIC) (Fig. 1.1e,f,g). Collections of these intercellular channels make up a gap junction plaque (Fig. 1.1j)[6; 7]. GJIC allows for direct cytoplasmic interaction between coupled cells[4].

Connexins are also known to communicate through non-junctional, channel independent mechanisms also known as the connexin interactome (Fig. 1.1h). In this type of communication, proteins bind to the intercellular regions of the connexin, either the carboxy or amino termini, creating proteincomplexes[8]. Interactions at extracellular connexin domains can also form adhesion domains (Fig. 1.1i). In this method of connexin communication, cells use connexins as migrational guides, such

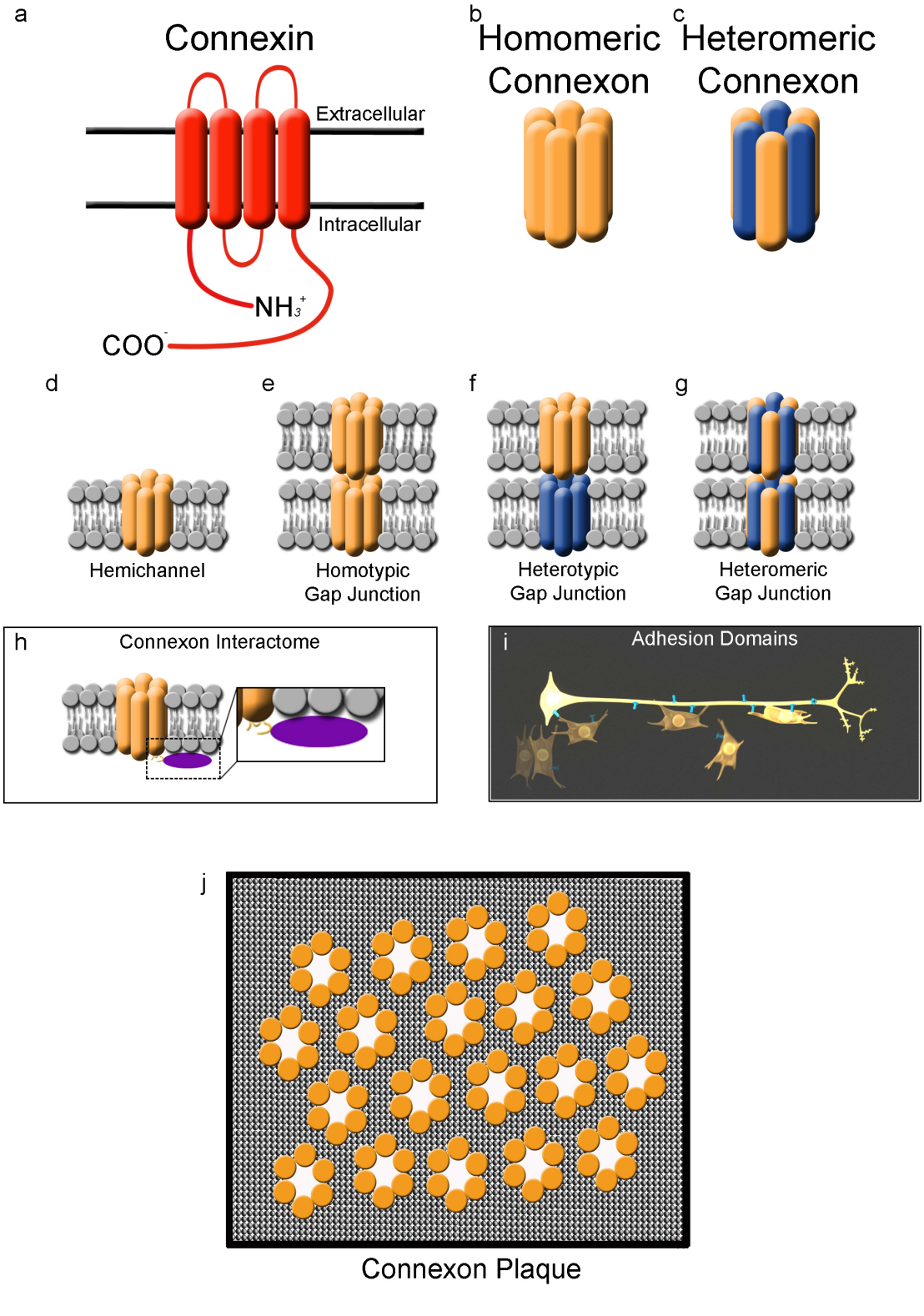
a
Connexin
Extracellular
Intracellular
NH3+
COO-
b
Homomeric
Connexon
c
Heteromeric
Connexon
d
Hemichannel
e
Homotypic
Gap Junction
f
Heterotypic
Gap Junction
g
Heteromeric
Gap Junction
h
Connexon Interactome
i
Adhesion Domains
j
Connexon Plaque

Figure 1.1 The connexin protein, connexons, and connexon mediated communication.

(a) The connexin protein consists of four transmembrane domains, two extracellular loops, one intracellular loop, and intracellular amino and carboxy termini. (b,c) Six connexins hexamerize to form a connexon. (b) Homomeric connexons are oligomers of the same connexin proteins, (c) and heteromeric connexons consist of different connexin proteins. (d) Hemichannels consist of a connexin oligomers communicating with the extracellular space. (e-g) Connexins aligning from adjoining cells form a gap junction and mediate GJIC. (e) Homotypic gap junctions are made up of two homomeric connexons. (f) Heterotypic gap junctions consist of two different homomeric connexons. (g) Heteromeric gap junctions consist of two heteromeric connexons. (h) The connexin interactome is when proteins interact with intracellular domains of the connexin protein. (i) Connexin communication through adhesion domains is when connexins are used as docking proteins for cellular movement. (j) Connexons congregate in cell membranes forming connexin plaques.

as cardiac neural crest cells utilizing connexin43 (Cx43) adhesion domains to migrate to final destination required for proper cardiac development[9].

There are 20 known connexons expressed in mice, and 21 expressed in humans[10]. Each connexon is named according to its corresponding molecular weight in kDa. A connexon/hemichannel can be composed of a single type of connexin, which is called a homomeric connexon (Fig. 1.1b), or different connexins making the connexon heteromeric (Fig. 1.1c)[3]. When two homomeric connexons align, forming an intercellular channel, the channel is known to be homotypic (Fig. 1.1e). When two different homomeric connexons align, the channel is known to be heterotypic (Fig. 1.1f). When two heteromeric connexons align the channel is known to be heteromeric (Fig. 1.1g)[3]. The type of connexins present in a connexon, and the type of gap junction channel formed (hemichannel, or homotypic, heterotypic, or heteromeric GJs) dictates channel specificity[6]. Moreover, connexin-mediated channels are gated in response to size selectivity, voltage, chemical stimuli, and pH[3; 6; 11; 12].

Connexon nomenclature has been described previously (reviewed in Sohl and Willecke 2003). Connexins are first named according to the species in which they were identified and by their molecular mass (kDa)[10]. For example mouse connexin36, the 36 kDa mouse connexin protein, would be assigned mCx36. Another naming system for connexins uses sequence similarity, length of cytoplasmic domains, and the order in which the connexin in a particular domain was discovered[10]. Connexins with similar sequences and cytoplasmic domains are grouped together into groups; α, β, γ[10]. This naming system is first designated with

the abbreviation Gj, for Gap Junction, then uses the α, β, or γ, to indicate the class in which the connexin falls, and finally the order in which the connexin was discovered[10]. mCx43, for example, is also designated GJa1 as the first α group-associated connexin discovered[10]. Interestingly for neuronal connexins, Cx45 and Cx36, novel groups of naming have also been proposed by Sohl and Willecke to describe their dendrogram/phylogenic tree[10]. Here, it is argued that Cx45, Cx47 and Cx36 should be taken out of the α-group due to their separation from the α-group in the dendrogram and phylogeny tree[10]. It is argued that Cx45 and Cx47 should be designated as part of the γ-group because of their cytoplasmic loop length similarities and sequence similarities[10]. Along the same lines, mCx36 or hCx36 should be in a novel δ divergent subgroup because of their unique sequence and cytoplasmic loop properties and thus grouped with other divergent connexins mCx29, Cx23, mCx39, and hCx40.1[10]. A complete list of mouse and human connexin and gap junction nomenclatures is provided in Table 1 (adapted from[10]).

1.2 Neuronal connexons.

Eleven connexins are detected in the central nervous system (CNS): Cx26, Cx29, Cx30, Cx32, Cx36, Cx37, Cx40, Cx43, Cx45, Cx47, and Cx57 [4; 13; 14]. Only Cx36, Cx45, and Cx57 are expressed by neurons, with Cx57 restricted to horizontal cells of the retina [3; 15; 16]. Neuronal connexins mainly form electrical synapses [3; 17; 18; 19], however they are known to be permeable to cAMP, ATP, and dyes such as neurobiotin and lucifer yellow [20; 21; 22; 23]. Cx36 can form hemichannels [21], homotypic gap junctions [3; 24], and heterotypic gap junctions with Cx45 [25].

Connexin Name (Cx)		Gap Junction Name (GJ)			
mCx	hCx	Former GJ name		Current GJ name	
		Mouse GJ	Human GJ	Mouse GJ	Human GJ
mCx23	hCx23	---	---	Gjd5	GJD5
x	hCx25	x	---	x	GJB7
mCx26	hCx26	Gjb2	GJB2	Gjb2	GJB2
mCx29	hCx30.2 (hCx31.3)	Gje1	GJE1	Gjd1	GJD1
mCx30	hCx30	Gjb6	GJB6	Gjb6	GJB6
mCx30.2	hCx31.9	Gja11	GJA11	Gjd3	GJD3
mCx30.3	hCx30.3	Gjb4	GJB4	Gjb4	GJB4
mCx31	hCx31	Gjb3	GJB3	Gjb3	GJB3
mCx32	hCx32	Gjb1	GJB1	Gjb1	GJB1
mCx33	x	Gja6	x	Gja6	x
mCx36	hCx36	Gja9	JGA9	Gjd2	GJD2
mCx37	hCx37	Gja4	GJA4	Gja4	GJA4
mCx39	hCx40.1	---	---	Gjd4	GJD4
mCx40	hCx40	Gja5	GJA5	Gja5	GJA5
mCx43	hCx43	Gja1	GJA1	Gja1	GJA1
mCx45	hCx45	Gja7	GJA7	Gjc1	GJC1
mCx46	hCx46	Gja3	GJA3	Gja3	GJA3
mCx47	hCx47	Gja12	GJA12	Gjc2	GJC2
mCx50	hCx50	Gja8	GJA8	Gja8	GJA8
mCx57	hCx62	Gja10	---	Gja10	GJA10
x	hCx59	x	GJA10	x	GJA9

Table 1.1 List of human and mouse connexin (Cx) names, including former and current gap junction (GJ) naming systems.

(x) designates no connexin present for that species. (---) designates no GJ name for that connexin.

Cx36 and Cx45 are developmentally regulated connexins. Both Cx36 and Cx45 are abundantly expressed throughout the developing rodent brain [16; 19; 26]. Expression of Cx36 is first observed on embryonic day 7.5 (E7.5), and is strongly detected by day E9.5 in the forebrain[27]. Expression levels increase as the mouse develops to postnatal day 14 (P14) until Cx36 is expressed throughout the murine brain[15; 26; 28]. In the cortex, Cx36 mRNA levels are abundant at P7 and become reduced to scattered cells into adulthood[26; 28]. In the adult hippocampus, Cx36 expression was thought to be restricted to interneurons of the stratum pyramidale[19; 28], but there is now evidence for protein expression in pyramidal neurons, at least in rat[29; 30]. Expression in mouse pyramidal neurons remains unclear and controversial[19; 29; 31]. In the adult rodent, Cx36 is found in the inferior olive, cerebellum, olfactory bulb, pineal gland, anterior pituitary, spinal cord, retinal inner and outer plexiform layer, and AII amacrine cells[28]. Similarly, Cx45 expression is found in nearly all brain regions during development[16]. Expression is dramatically reduced in hippocampus, cortex, striatum, thalamus and cerebellum in the adult brain and is restricted to NeuN-positive neurons [16].

1.3 Lessons learned from Cx36 null-mutant mice.

In the $Cx36^{-/-}$ mouse developed by Dr David Paul, a biscistronic cassette containing both placental alkaline phosphatase (PLAP) and LacZ reporter genes replaces the Cx36 coding sequence under endogenous control of the Cx36 promoter[32]. Phenotypically, Cx36 null mutant mice display no gross deficits in motor performance[3; 33]. However, because inferior olive neurons are coupled by Cx36, knockout mice have abolished subthreshold oscillation synchrony[34]. The loss of

spike synchrony in inferior olivary neurons in Cx36$^{-/-}$ mice adds 10 – 20 ms to temporal coordination of muscle firing, thereby affecting fine motor tasks[35]. In the hippocampus, which plays an important role in learning and memory, Cx36 expression has only been detected in GABAergic interneurons in mice[19] despite reports to the contrary in rats[29; 30]. Cx36$^{-/-}$ mice show deficits in object recognition in a new object recognition task[36]. In wild-type mice, fear-motivated learning and memory can be hindered by stereotactic injections of gap junction blockers carbenoxolone and mefloquine into the dorsal hippocampus[37]. Although carbenoxolone is a broad pan-connexin channel inhibitor, mefloquine is a more specific inhibitor of Cx36-mediated channels[38]. Ablation of Cx36 from hippocampal interneuron populations disrupts kainate induced gamma frequency network oscillations in vivo[39] and in vitro[19]. Cx36$^{-/-}$ mice have a reduction in γ-oscillation rhythmicity, and inhibitory post synaptic potentials (IPSPs) are disrupted in both amplitude and rhythmicity [19]. Hippocampal interneuron coupling is abolished in Cx36$^{-/-}$ mice [19]. High frequency oscillations remain unaffected by the loss of Cx36 [19; 39], giving rise to the possibility that excitatory pyramidal neurons are coupled by another gap junction [28]. The differentiation of excitatory pyramidal cell and inhibitory interneuron networks may enable the proper entrainment of pyramidal cell discharges through modulatory GABAergic interneuron influence [28]. Somewhat surprisingly, Cx36$^{-/-}$ mice exhibit differences in pyramidal NMDA receptor (NMDAR) subunit protein expression compared to wild-type mice (despite the fact that protein has not been detected in mice, although recent reports suggest that rats may express Cx36 in pyramidal neurons)[29; 30]. The NMDAR subunit ratio NR2A/NR2B is

greater in the hippocampus of $Cx36^{-/-}$ mice compared to $Cx36^{+/+}$ mice[40], indicating (a) there may be a developmental effect of Cx36 in regulating NMDAR subunit expression required for adult distribution and (b) there may be possible variations in excitotoxic mediated damage between the genotypes. NMDARs are primary mediators of glutamatergic excitotoxic damage, which can be caused by neurodegenerative conditions such as epilepsy. In humans mutations in the Cx36 gene have been associated with juvenile myoclonic epilepsy[41].

1.4 Connexins influence cerebral excitotoxic damage and disease.

During stroke (ischemia), blood flow is restricted or stopped resulting in oxygen and glucose deprivation that is required for normal cell function. In the area surrounding the stroke, an accumulation of Ca^{2+} in relation to the necrotic lesion core initiates death pathways associated with excitotoxicity[42; 43]. Connexins are implicated in transmission of this injury. $Cx43^{+/-}$ mice exhibit a larger infarct volume compared to wild-type, suggesting that the presence of Cx43 is protective against stroke associated cellular injury and death[43]. The propagation of cell death observed around the central "stroked area" is known as the "bystander effect"[44]. The "bystander effect" of cell death is not only observed in ischemia, but in other models of disease and trauma[44]. There is a growing body of evidence suggesting that GJIC represents one means of propagating cell death second messengers such as Ca^{2+} through clusters of coupled cells[45; 46; 47]. In support of this hypothesis, GJIC blockade with the pharmacological inhibitor carbonoxolone, or 18-β-glycyrrhetinic acid can prevent apoptosis[45; 48; 49; 50].

1.5 Kainic acid (KA)-induced excitotoxicity.

Excitotoxicity refers to the damage and death caused to neurons following excessive release of excitatory neurotransmitters, such as glutamate. Sustained glutamatergic neurotransmission causes overactivation of ionotropic glutamate receptors. Damage underlies neuronal loss in diseases such as epilepsy, Alzheimer disease (AD), cerebral ischemia and Parkinson's disease (PD)[51]. Temporal lobe epilepsy (TLE) is a chronic condition, and is the most common form of human epilepsy[52]. It is postulated TLE is caused by dysregulation of inhibition and excitation, causing synchronous overactivation of excitatory neurons[53]. In kindling models, TLE can be induced by the chronic activation of KA receptors. Acute animal models of kainate-induced seizure (i.e., systemic injection of KA) can also be employed to observe neuronal survival, recovery, or susceptibility to damage. These acute animal seizure models have also proven useful in drug discovery[54].

KA is an analog of glutamate[55], and is derived from a red algae called *Digenea simplex* [51]. The use of KA is an established model of excitotoxicity[51; 56]. KA is known to bind kainate receptors, which are predominantly located in the *cornu ammonis* 3 (CA3) region of the hippocampus, with fewer being found in the CA1 region[56; 57]. Following kainate administration, neurons in the CA1, and more principally in the CA3 region of the hippocampus, experience delayed cell death in rodent models[51]. Neuronal cell replacement in the damaged CA3 region of the hippocampus is limited post injury in wild-type mice[58]. Kainate receptors are a class of ionotropic glutamate receptors. Ionotropic glutamate receptors are grouped as N-methyl-D-Aspartate (NMDA) and non-NMDA receptors, which include kainate and L-α-amino-3-hydroxy-5-methylisoxazole-4-propionate receptors (AMPAR)[57]. As the

name ionotropic glutamate receptor implies, these receptors all are able to bind glutamate and play a role in excitotoxicity. NMDARs consist of NMDA subunits NR1, and NR2A-D [59]. AMPARs consist of subunits GluR1-4, and kainate receptors consist of subunits GluR5-7 and KA1-2[56; 57]. CA3 pyramidal cells are particularly sensitive to KA[60]. Upon binding of KA, there is a cellular influx of Ca^{2+} which can lead to the activation of various enzymes including endonucleases, phospholipases, proteases, the activation of reactive oxygen species (ROS) causing mitochondrial dysfunction, and the activation of apoptotic, or necrotic pathways (Fig. 1.2)[51]. Further, extrasynaptic NR2B receptors have reportedly been the main effector of excitotoxic injury post ischemia in neurons[61]. In the days following kainic insult, degenerating cells are stained with *in situ* nick end labeling, again suggesting apoptosis and necrosis pathway activation[51]. Activated microglia have been shown to be recruited to the damaged CA3 region of KA injured rats five days post administration, highlighting the importance of glial cell activation and neuronal cell death following excitotoxic injury[51].

1.6 The role of microglia following excitotoxicity.

Microglia are the resident immune cells of the CNS, and consist of approximately 10% of the CNS cell population[62]. Relevant to this thesis, they are the only cell type (other than neurons) known to express Cx36[63]. They are responsible for removal and clearance of unwanted cells, or debris. Microglia reside throughout the brain and spinal cord in an inactive state as ramified microglia[62]. Morphology is defined by a small cell body with long protruding extensions (Fig. 1.3a). It is thought that these inactive microglia roam the CNS in search of foreign invaders, cellular

damage, or debris such as plaques[64]. The long projections of ramified microglia scan surrounding areas for unwanted material, and upon finding damaged cells, invaders, or foreign debris they become activated[64]. When microglia become activated their processes retract and cell bodies become larger reaching an amoeboid state where they actively contact damaged or unwanted cells and debris, which they can phagocytose (Fig. 1.3a-d)[62; 65]. Activated microglia express Iba1, upregulated during the activation process[66]. Microglia eliminate unwanted CNS invaders through phagocytotic and cytotoxic mechanisms[67]. Microglia can also act as antigen presenting cells, and can release factors such as pro-inflammatory cytokines, heat shock proteins, and acute phase proteins which increase the cerebral immune response[68].

Following administration of KA, there are observed increases in microglia cell number in the CA3 region of the hippocampus[51]. Activation of microglia is commonly associated with neurodegeneration processes, and contribute to increases observed in proinflammatory factors and reactive oxygen species (ROS)[51]. Microglia can release large quantities of cytotoxic substances[69]. In *in vitro* experiments, it was observed that microglia release H_2O_2, nitric oxide (NO), glutamate and aspartate[70; 71; 72]. In experiments utilizing rat cerebral cortex neuronal- microglia co-cultures, observed cell contact and phagocytosis incurred large amounts of neural death which the authors suggest is mediated by H_2O_2[73]. The Spray lab has verified a direct cell-cell coupling mediated by Cx36 between neurons and microglia through electrophysiology and dye transfer studies[63]. Further, it has been reported that activated microglia can cause the focal destruction of damaged neurons through the direct release of Ca^{2+} stores[74]. Thus, I hypothesize that during excitotoxic conditions

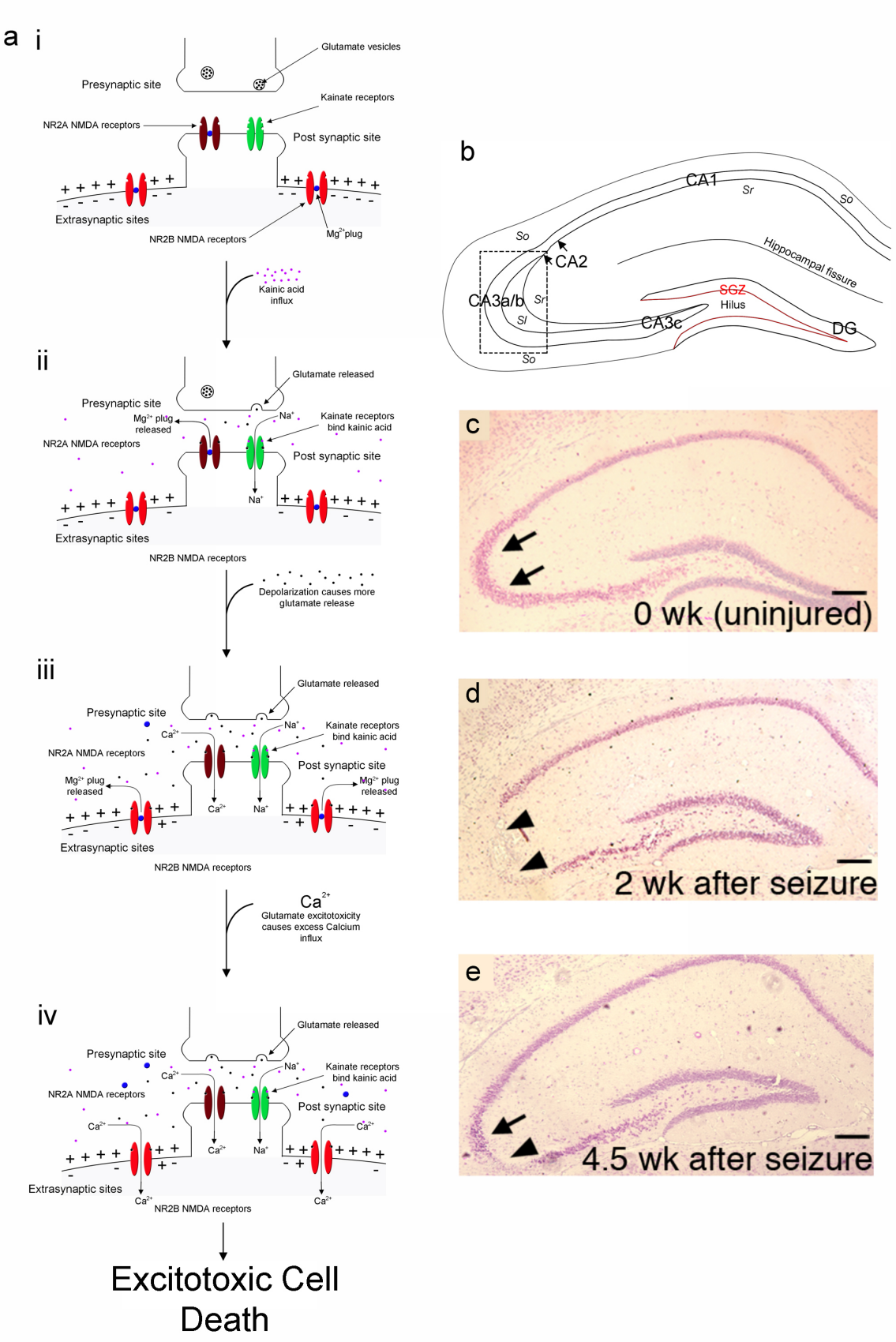
a
i
Glutamate vesicles
Presynaptic site
Kainate receptors
NR2A NMDA receptors
Post synaptic site
Extrasynaptic sites
NR2B NMDA receptors
Mg2+plug
Kainic acid influx
ii
Glutamate released
Presynaptic site
Mg2+ plug released
Na+
Kainate receptors bind kainic acid
NR2A NMDA receptors
Post synaptic site
Extrasynaptic sites
NR2B NMDA receptors
Depolarization causes more glutamate release
iii
Glutamate released
Presynaptic site
Ca2+
Na+
Kainate receptors bind kainic acid
NR2A NMDA receptors
Post synaptic site
Mg2+ plug released
Mg2+ plug released
Extrasynaptic sites
NR2B NMDA receptors
Ca2+
Glutamate excitotoxicity causes excess Calcium influx
iv
Glutamate released
Presynaptic site
Ca2+
Na+
Kainate receptors bind kainic acid
NR2A NMDA receptors
Post synaptic site
Ca2+
Ca2+
Extrasynaptic sites
Ca2+
NR2B NMDA receptors
Ca2+
Excitotoxic Cell Death
b
CA1
Sr
So
So
CA2
Hippocampal fissure
SGZ
Hilus
CA3a/b
Sr
Sl
CA3c
DG
So
c
0 wk (uninjured)
d
2 wk after seizure
e
4.5 wk after seizure

Figure 1.2 The KA model of excitotoxic injury.

Kainate receptors are primarily located in the CA3a/b region of the hippocampus (b, dotted box; c, arrows). Upon sufficient binding of KA to kainate receptors, regional membrane depolarization is observed (a,i-ii). Depolarization releases Mg^{2+} blocking the NMDAR pores leading to threshold depolarization and sustained neuronal firing (a,iii). With depolarization, the quanta of glutamate released in the synaptic cleft is enhanced and the cycle continues causing the observed excitotoxic cellular damage in the hippocampus (a,iv). CA3a/b delayed excitotoxic cell loss is observed (d), and limited cell replacement is observed four weeks post KA-injury (e). Photomicrographs are from the Bennett laboratory of methyl-green pyronin Y stained sections of wild-type C57BL/6 mice (N12) sacrificed at the indicated times following KA. Scale bar, 50 μm.

activated microglia could instigate the death of damaged neurons through the coupling of these cell types, mediated by Cx36, and the direct passage of Ca^{2+}. The coupling of damaged neurons and activated microglia could also instigate the propagation of Ca^{2+} waves, which would depolarize these cells and cause the release of more glutamate[75]. This could provide insight into a link between excitotoxic mediated neuronal death with microglia, either through direct GJIC or microglial hemichannels, which has yet to be elucidated *in vivo* and *in vitro*. During periods of excitotoxic insult such as NO dependent excitotoxicity, ischemia, and Alzheimer Disease (AD), microglia have been found to have neuroprotective properties[68; 76; 77]. However during periods of overstimulation, overactivation, or dysregulation, microglia can become harmful and have negative outcomes on neurons and their environment making them potentially attractive targets for therapeutic intervention[78].

1.7 Relationship between Cx36 and excitotoxicity.

In the kainate receptor-rich CA3 region of the hippocampus, expression of Cx36 is limited to interneurons of the pyramidal cell field including the stratum *radiatum* and *stratum oriens* in adult mice[19]. Following KA administration Cx36 expression is known to be downregulated 48 hours post injury[79]. In rats four weeks post injury in both kainate treated and kindling models, there was no observed difference in Cx36 protein expression in the CA3 region of the hippocampus[80]. Intriguingly, NMDAR-dependent cell death in mice, both in terms of NMDAR hyperfunction and hypofunction, require Cx36[48]. In the absence of Cx36, murine hypothalamic cultures do not die from NMDAR hyperfunction or hypofunction[48]. It is

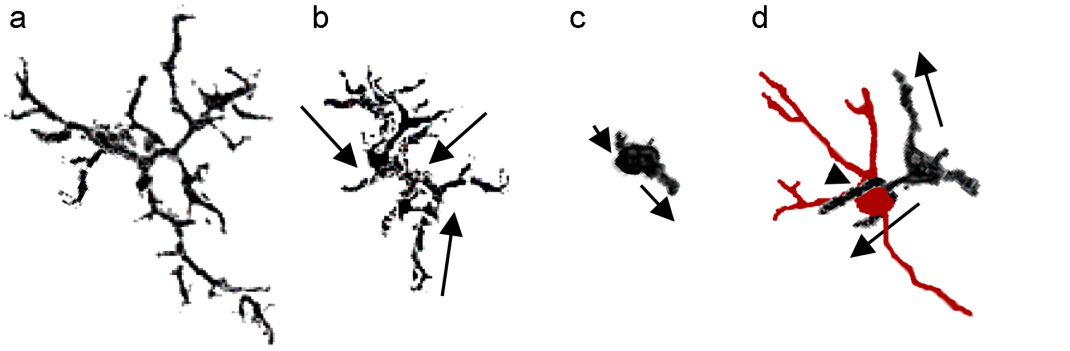
a
b
c
d
Ramified
Ramified with processes retracting
Ameboid
Ameboid with process extensions

Figure 1.3 Changes in microglial morphology over the course of activation.

Microglia are dynamic cells that can switch from resting (ramified) to activated (amoeboid) states. Ramified microglia have long processes (a), as they become activated their processes retract (b). Ameoboid or activated microglia loose their processes (c), and can extend new ones to contact cells/debris (d). Red cell indicates a dying or damaged cell actively being contacted or phagocytosed by an activated microglia (black cell).

also known that NMDAR antagonists administered before or after KA induced injury prevent most of the excitotoxic damage normally observed[56].

1.8 Electrophysiology – KA and Cx36.

The use of KA in hippocampal electrophysiology slice experiments with $Cx36^{-/-}$ and $Cx36^{+/+}$ animals has been performed to elicit the release of physiological levels of glutamate, and observe the burst firing frequency variations in the absence of Cx36[19]. Cerebral inhibitory interneurons located in thalamic reticular nuclei, inferior olive, cerebellum, retinal neurons, cortex, and hippocampus, including the CA1 and CA3 regions are known to express the electrical synaptic protein Cx36[3; 19; 81; 82]. Interneurons synchronously fire at all frequencies because of their electrical coupling through Cx36[19; 82]. Electrical coupling and cell spiking is divided into a number of categories, namely theta oscillations (~9-12Hz), gamma oscillations (~30-80Hz), and super fast oscillations (>100Hz), also known as ripples[19; 39]. In the absence of Cx36, theta oscillations, and high frequency ripples are unaffected, however gamma oscillations are no longer synchronous[19; 39]. By knocking out Cx36 a reduction in amplitude and rhythmicity in IPSPs is observed in both pyramidal cells and interneurons in kainate treated hippocampal slices[19]. The disruption of γ-oscillations and alterations observed in IPSPs in excitatory hippocampal networks highlight the importance of Cx36 in the inhibitory GABAergic interneuronal communication, and the influence that these cells have on entire networks of excitatory pyramidal cells during excitotoxic events. While the use of slice preparations has been done to assess the functionality of damaged hippocampi, to

date slice preparations have not been used to assess the functionality of hippocampal formations post KA-injury.

1.9 Rationale, hypothesis, objectives.

The relationship between neuronal Cx36 and excitotoxic brain injury is not fully understood. Based on the evidence described above, I hypothesized that Cx36 mediated communication, either though GJIC or hemichannels, participates in mediating excitotoxic cell death in the hippocampus following KA induced injury. I hypothesize that, in the absence of Cx36, excitotoxic neuronal injury will be reduced. To test these hypotheses and provide mechanistic insight into the role of Cx36 in propagating seizure injury, I employed a loss of function approach, using Cx36 knock out mice, to assess whether loss of Cx36 was indeed protective in the hippocampus following KA-induced excitotoxic challenge. Here, I address three specific aims:

(1) Assess the extent of KA-induced excitotoxic damage in the CA3 region of the hippocampus in $Cx36^{+/+}$ and $Cx36^{-/-}$ mice.

(2) Determine how loss of Cx36 alters CA3 pyramidal neuronal response to KA.

(3) Determine if CA3 pyramidal cells in $Cx36^{-/-}$ mice are functional following excitotoxic insult.

2. Chapter 2 – Materials and Methods

2.1 Animals.

All experimental protocols were approved by the Animal Care Committee of the University of Ottawa according to guidelines set forth by the Canadian Council on Animal Care. $Cx36^{-/-}$ mice on a C57BL6/129SvEv hybrid background were generated as previously described[82]. Mice were backbred for four generations (N4) onto a C57Bl/6 lineage in the Bennett laboratory and compared to congenic N4 $Cx36^{+/+}$ wild-type littermates derived from mating of heterozygote breeding pairs. Mice were kept on a 12 h light-dark cycle with food and water available *ad libitum*. Animals were genotyped both at weaning and upon sacrifice. An overnight digestion of ear samples was performed at 55°C in digestion buffer (100 mM Tris-Cl pH 8.5, 5 mM EDTA, 200 mM NaCl, 0.2% SDS) with 20.8 mg/ml proteinase K (Wisent, CA# 800-030-EM). DNA from digested tissue was extracted in phenol chloroform/isoamyl alcohol and precipitated using isopropanol. DNA was resuspended in 150 ml of Tris-Ethanolamine (TE) buffer (10 mM Tris-Cl pH 7.5, 1 mM EDTA). PCR analysis was performed using primers designed to amplify a $Cx36^{+/+}$ band (5'-AGCGGAGGGAGCAAACGAGAAG-3', and 5'- CTGCCGAAATTGGGAACACTGAC-3', generating a 533 bp product), and a $Cx36^{-/-}$ band (5'-GGTGAACCGCAACTGGTACT-3; and 5'-CCCACCTTGGCTGTAGTCAT-3', generating a 187 bp product). PCR analysis was performed using a BioMetra (TGradient) thermocycler. Cycling time for the $Cx36^{+/+}$ reaction was 94°C for 1 minute, followed by 30 cycles of 94°C of 15 seconds, 69°C for 15 seconds, 72°C for 45 seconds, and then held at 4°C. Cycling time for the $Cx36^{-/-}$ reaction was 95°C for

15 minutes, then 35 cycles of 95°C for 30 seconds, 63°C for 90 seconds, 72°C for 2 minutes, followed with one cycle of 72°C for 15 minutes, and a 4°C hold.

2.2 Tissue preparation.

A total of n=73 $Cx36^{+/+}$ and n=51 $Cx36^{-/-}$ mice were sacrificed by lethal injection with sodium pentobarbital during this study. Mice were transcardially perfused with 10 mM phosphate buffered saline (PBS; 10 mM sodium phosphate, 154 mM sodium chloride, pH 7.2) followed by 4% formaldehyde (Sigma, CA# F1635) in 10 mM PBS. Neonatal and adult mice were assessed at 1 week of age or 2.5-3 months of age respectively. Brains were removed, post-fixed for 24 h in the same fixative, and cryoprotected in 20% sucrose solution in 10 mM PBS containing 0.001% NaN_3, for 48 hr at 4°C.

For *in situ* hybridization, all reagents were diethylpyrocarbonate (DEPC, Sigma, CA# D5758)-treated prior to perfusion, fixation, and cryoprotection and all equipment was cleaned with RNAse Away (Invitrogen, CA# 10328-011). Tissue was flash-frozen and serial coronal or sagittal sections (10 µm thickness) were prepared using a Leica CM1900 cryostat (Leica Microsystems Inc., Richmond Hill, ON). Sections were stored in RNAse-away-treated slide boxes with desiccate bags to minimize condensation.

For quantitative immmunofluorescent analyses, tissue was prepared for serial counts (interneuronal counts) in the following manner. Serial 30 µm and 10 µm coronal sections were collected (Leica Microsystems, Wetzlar, Germany) through the whole hippocampus (bregma -0.80 to -4.30 mm). Thirty µm sections were collected for the first five sections and placed in incremental wells of a 12 well plate

containing 0.1M PBS + 0.1% sodium azide (NaN_3). The cryostat was changed to a 10 µm thickness and three sections were taken and mounted on a slide (Superfrost/Plus, Fisher, catalog # 12-550-15). The process was repeated five times (with three sections/slide). The crysostat was then reset to collect 30 µm sections and the process commenced from the beginning. Thus 30 µm sections were collected in a 1 in 10 series. Free floating (30 µm) sections were stored at 4ºC. The 10 µm slide-mounted sections were stored at -80ºC.

2.3 KA-induced seizures.

Adult mice (3 months of age) received single intraperitoneal injections of 15 mg/kg KA (Sigma, CA# K250). Seizure intensity was assessed based on a five-point behavioural scale as previously described[83]: 0, no response; 1, reduced locomotion and sedation; 2, automatisms including head bobbing, scratching, repetitive face washing, increased frequency of "freezing" and "wet-dog shakes"; 3, tremors and weak clonic convulsions; 4, intermittent followed by continuous rearing with forelimb clonus and loss of postural control; and 5, severe limbic seizures with respiratory difficulty. Within five minutes of reaching status epilepticus (stage 4 seizure), animals received 5 mg/kg of diazepam to limit convulsions and were placed in housing under reduced light and minimal sound. Animals were kept under close observation for 6 hr to monitor additional seizure activity. Only mice that reached stage 4 were used. Mice were euthanized with sodium pentobarbital 3, 7 or 28 days following KA-induced seizure and transcardially perfused with 10 mM PBS and 4% paraformaldehyde in 10 mM PBS as described above.

2.4 In situ hybridization.

Cx36 mRNA expression was analyzed in neonatal (1 week of age) and adult mice (2.5-3 months of age). *In situ* hybridization was performed as described previously [84] using two digoxigenin (DIG)-labelled anti-sense oligonucleotides: 5' GGTGGTCTCTGTGTTCTGCAGCACCCCATTGACCATGGC-3' and 5'-CTGGGCTCCCCGGACAGCCAGTTTGATCTTCCGCCAT-3' [19]. DIG-labelled oligonucleotides were synthesized by Integrated DNA Technologies. Briefly, all surfaces in contact with slides were cleaned with RNase away. Sections were removed from stored slide box in -20ºC environment and placed in a chamber containing desiccate (Drierite, W.A. Hammond Drierite Company LTD., Ohio, USA) and allowed to acclimatize to room temperature in chamber for 30 minutes to minimize condensation. Sections were hybridized overnight at 65°C in humidity chambers containing 50% formamide (EMD chemicals, Darmstadt, Germany) in a 1X salt solution (20 mM NaCl, 9 mM Tris-HCL, 1 mM Tris base, 5 mM dihydrous sodium phosphate, 5 mM disodium phosphate and 5mM EDTA) on filter paper. Both probes were used at 100 pg/ml in a 1:1 mixture in hybridization buffer (50% deionized formamide, 20% of a 50% dextran sulfate solution, 0.1 mg/ml yeast rRNA, 1X Denhardt's solution (2% bovine serum albumin, 2% Ficoll 400, 2% polyvinyl pyrolidone) in a 1X salt solution). Sections were washed four times at 65°C in 1X Maleic Acid Buffer containing 0.1% Tween-20 (MABT; 0.1M maleic acid, 0.16M NaOH, 0.15M NaCl, 0.1% Tween-20) and incubated for 1 h at room temperature in blocking solution (20% sheep serum, 2% blocking reagent (Roche, CA# 1096176), in 1X MABT). Signal was detected using anti-DIG-alkaline phosphatase (Roche, CA# 11093274910, 1:1500) diluted in blocking solution and incubated at 4°C

overnight. Sections received four 20-min washes in 1X MABT and two 10-min washes in pre-staining solution (100 mM NaCl, 100 mM Tris-Cl pH 9.5, 50 mM $MgCl_2$, 0.1% tween-20). Following the pre-staining washes sections were placed in staining buffer (100 mM NaCl, 100 mM Tris-Cl pH 9.5, 50 mM MgCl2, 0.1% Tween-20, 10% polyvinvyl alcohol) containing 4-Nitro blue tetrazolium chloride (NBT; Roche, CA# 11383213001) and 5-bromo-4-chloro-3-indoyl-phosphate (BCIP; Roche, CA# 11383221001) and incubated overnight. After staining, sections received four 10-min washes in 10 mM PBS, were dehydrated, and coverslipped using DPX (Fluka, CA# 44581).

2.5 Histology, immunofluorescence and cell counts.

Haematoxylin & eosin (H&E) staining was used to qualitatively assess neurodegeneration following excitotoxic injury. For immunofluorescence, primary antibodies were: mouse anti-NeuN (Chemicon; CA# MAB337; 1:50), mouse anti-parvalbumin (Sigma, CA# P3088; 1:1000), rabbit anti-parvalbumin (Swant, CA# PV-28; 1:1000), mouse-anti-connexin36 (Millipore, CA# MAB3045; 1:100), rabbit anti-Iba1 (Wako, CA# 019-19741; 1:100). Secondary antibodies include Cy3-conjugated donkey anti-mouse IgG (Jackson, CA# 715-165-150; 1:400), FITC-conjugated donkey anti-mouse IgG (Jackson, CA# 715-095-150; 1:50), Cy3-conjugated donkey anti-rabbit IgG (Jackson, CA# 711-166-152; 1:600), FITC-conjugated donkey anti-rabbit IgG (Jackson, CA# 711-096-152; 1:100). Prior to application of the primary antibody, slide mounted tissue was placed in 10 mM PBS for 5 minutes. Antibodies were diluted in antibody buffer (3% bovine serum albumin, 0.3% Triton X-100 in 10 mM PBS). Primary antibodies were applied to slide mounted tissue and a parafilm

cover slip was placed over tissue, evenly distributing the antibody and preventing antibody solution evaporation. Tissue was incubated at 4°C overnight. The following day, three 5 minute washes in 10 mM PBS were performed followed by a 1 hr incubation with secondary antibodies. Secondary antibodies were diluted in 3% bovine serum albumin, 0.3% Triton X-100, all in 10 mM PBS, and a parafilm cover slip was placed over tissue to evenly distribute antibody. Following secondary antibody incubation one 5 minute 10 mM PBS wash was performed, followed by one 5 minute incubation with nuclear stain Draq5 (Cell Signaling, CA# 40845; 1:1000 in 10 mM PBS) followed by one 5 minute 10 mM PBS wash. Following washes, sections were coverslipped in an “antifade” mounting media (Prolong Gold, Invitrogen, CA# P36930). Confocal laser scanning microscopy, Leica TCS Sp5 (Leica Microsystems), was used to identify immunopositive cells in z-stacks captured with Leica LAS AF software (version 2.41) using an HCX PL APO CS 63X 1.4 oil objective with a pinhole size of 1 Airy unit (or equal optical slices for multiple fluorophores). Immunopositive cells were also observed, and counted using immunofluorescence microscopy on a Leica DMXRA2 widefield microscope using a Hamamatsu Orca ER digital camera.

Free-floating tissue for stereology were prepared in the following manner; A well of sections representing 1 in 10 sections throughout the hippocampus (bregma -0.80 mm to -4.60 mm, 30 μm thick) were taken from storage media an floated in 10 mM PBS for 10 minutes. Tissue was then transferred to medium (3% bovine serum albumin, 0.3% Triton X-100 in 10 mM PBS) with diluted antibody and placed on shaker (S-500 orbital shaker, VWR, CA# 14005-830) at 4ºC overnight. Tissue was

then transferred to a series of two 10 minute 10 mM PBS washes with agitation on a platform shaker (The Belly Dancer, Stovall, model # USBDbo) at speed 7. Following the two PBS washes the tissue was transferred to media (3% bovine serum albumin, 0.3% Triton X-100 in 10 mM PBS) containing diluted secondary antibody with conjugated fluorophores and agitated on a platform shaker (The Belly Dancer, Stovall, model # USBDbo) at speed 7 for 1 hour and 10 minutes. Tissue was then transferred into 10 mM PBS and agitated on platform shaker at speed 7 for 10 minutes and this washing step was repeated. During secondary incubation and two subsequent washing steps, tissue was covered with tin foil in order to minimize exposure of the tissue to light and subsequent fluorescence degradation. Following the second wash hippocampal tissue was mounted on a slide and coverslipped using Prolong Gold mounting media containing DAPI (Invitrogen, CA#P36931). Cell counts were performed using Image J analysis software (NIH) [85]. The total number of labeled cells in a given region per animal was calculated as the sum of the cell counts in all sampled sections multiplied by the total number of serial sections collected and divided by the number of sections sampled as previously described[86; 87; 88].

In some cases, cells were quantified using the optical dissector method by counting cells in defined hippocampal subregions positive for NeuN in bilateral hippocampi in two adjacent 10 μm sections (n=4 hippocampi per animal) between dorsal bregma -1.60 mm to -2.10 mm. The region of the hippocampus assessed was an area that encompassed most medial tip of the CA3c. The measurement feature of OpenLab v5.08 software was used to determine the total area (mm^2) of each region and two independent investigators performed counts. Values were averaged

to produce a single value per animal and the data was expressed as the number of NeuN positive cells per 0.1 mm^2.

2.6 Terminal deoxynucleotidyl transferase dUTP nick end labeling (TUNEL).

Apoptotic cell loss and DNA damge was assessed by TUNEL (Roche, CA# 1684795). Sections were incubated for 5 min in 0.1% Triton-X/0.1% sodium citrate on ice, and a 2 min incubation in ethanol:acetic acid (2:1) on ice to permeabilize tissue. The sections then underwent a 2 min wash in 10 mM PBS, and were incubated in a humidity chamber for 1 hr at 37°C with fluorescein isothyanate (FITC)-labeled dUTP in TdT buffer (30 mM Tris-HCl, pH 7.2, 140 mM sodium cacodylate, 1 mM cobalt chloride) and TdT in accordance with the Roche protocol. Assessment of the number of apoptotic TUNEL-labelled cells in the hippocampus was as quantified by taking a total count number of two adjacent 10 μm sections including both bilateral hippocampi (n=4 hippocampi per animal) in the dorsal hippocampal region between bregma -1.60 mm to -2.10 mm. The CA3a/b region (medial tip) of the hippocampus was counted. Two independent investigators performed counts, and an average of the counts were taken. OpenLab v5.08 measurement feature was used to determine the total area (mm^2) of the regions assessed, and final $TUNEL^+$ cell counts were expressed per 0.1 mm^2.

2.7 Western analysis.

Hippocampi were dissected in sterile 10 mM PBS (pH 7.2) containing 10 mM sodium orthovanadate, 10 mM sodium fluoride, and 5.74 mM PMSF on ice using a Leica MZ6 dissecting microscope. To enrich for integral membrane proteins, tissue was placed in 300 ml TEVP buffer (20 mM Tris-Cl pH 7.4, 5 mM EDTA, 1 mM EGTA,

10 mM NaF, 2 mM Na_3VO_4, 1.5 mM PMSF, Complete EDTA-free protease inhibitor mini-tablet, Roche CA# 04693132001 in 10 ml of buffer) on ice, sonicated four times for 5 seconds using a F60 Sonicator Dismembrator (Fisher Scientific) at power 10, and centrifuged at 4000 gravitational-force units (x g) for 15 min followed by 16100 x g for 45 min at 4°C. The membrane pellet was solubilized in 200 ml TEVP buffer containing detergent (TEVP buffer including, 0.1% SDS (sodium dodecyl sulfate), 0.1% Na-deoxycholate, 1% NP-40) before centrifugation at 16100 x g at 4°C for 2 min. Supernatant was aliquoted and stored at -80°C. Protein concentration was determined using the Bio-Rad DC protein assay assay kit (BioRad; reagent A CA# 500-0113, reagent B CA# 500-0114, reagent S CA# 500-0115) according to manufacturer's protocol. Protein samples (10 µg) were separated on NuPage Bis-Tris 4-12% gels (NuPAGE, CA# NP0321BOX) using NuPage MOPS SDS running buffer (NuPage, CA# NP0001) and transferred to polyvinylidene difluoride membrane (Millipore, CA# IPVH00010). Membranes were blocked overnight at 4°C in 5% milk (Carnation, fat-free powdered milk) solution made in 0.1% 10 mM PBS-tween (0.1% indicating tween content) before overnight incubation at 4°C in primary antibodies. Primary antibodies used were rabbit anti-NR1 (Cell Signaling, CA# 5704; 1:1000), mouse anti-NR2B (Lifespan Biosciences, CA# LS-C16904; 1:750), mouse anti-NR2A (Lifespan Bioscience, CA# LS-C16900; 1:750), rabbit anti-GluR1 (Millipore, CA# 04-855; 1:2000), rabbit anti-GluR2/3/4 (Cell Signalling, CA# 2460; 1:1000), mouse anti-PSD95 (Fisher, CA# MA1-046; 1:12000), mouse anti-flotillin (BD Transduction Laboratories, CA# 610820; 1:12,000), and mouse anti-Na^+K^+ATPase-B2 (Millipore, CA# 05-369; 1:10000). Secondary antibodies used were peroxidase-conjugated donkey anti-rabbit IgG (Jackson Immunoresearch, CA#

711-035-152; 1:2000) or peroxidase-conjugated goat anti-mouse IgG (Jackson Immunoresearch, CA# 115-035-146; 1:2000). Antibodies were diluted in 5% milk solution made in 0.1% 10 mM PBS-tween. Immunolabeling was visualized using ECL detection reagents, SuperSignal West Pico Chemiluminescent Substrate Kit (Thermo Scientific, CA# 34080). Densitometry was performed using Image J analysis software v1.47m (NIH)[85].

2.8 Morris Water Maze.

Learning and memory were assessed using the Morris Water Maze (MWM) (Med Associates Inc., Water maze pool – mouse, CA# ENV-514M-B). Mice were placed in a pool with opaque white water, coloured with white non-toxic liquid tempera paint. Pool dimensions were 134.5 cm in diameter, and 53.3 cm deep with a floor insert. A platform (10 cm in diameter) was located in the center of the back right quadrant of the pool 1 cm below the surface of the opaque water, not visible to mice swimming in the pool. Visual cues were placed within visual range of the mice, a “square” to the left, and an “X” to the front of the pool (in relation to the four designated front-left, front-right, back-left, and back-right quadrants). The testing area dimensions were 2.98 m x 3.97 m x 2.62 m (LxWxH) respectively. Prior to testing mice were singly housed for 28 days. The mouse cages were changed (fresh food/bedding/water) the day before testing and then left untouched until completion of the MWM. Mice were first placed in the MWM behaviour room one hour prior to MWM testing. To ensure there are no auditory disturbances over the course of the behavioural testing 60 min prior to testing, mice are exposed to white noise using a white noise generator (San Diego Instruments, Serial # SDI 000141) set to 70 dB.

This noise is left on for the duration of the MWM testing. Water temperature of pool and room is maintained at 21ºC. Room light intensity at pool level and where mice are housed is checked using a Light meter (ExTech, light meter 401025), to ensure a steady illumination of 100 lux. Different cohorts were tested for eight days with four trials per day at zeitgeiber 9 (mice were tested 9 hours after lights on, based on 12 hour lights on, 12 hour lights off schedule). Mice were introduced to the pools and allowed to search for the platform for up to 1 minute. In each trial. mice were arbitrarily placed in the 4 different zones through the trials. Placements were randomly selected as front left, front right, back left, and back right zones. If the mouse did not find the platform within the one minute trial the experimenter indicated to the subject the platform location by site-specific tapping for ten seconds so that the mouse visually saw, and audibly heard, where the platform was located. If the mouse did not come to the platform, the experimenter manually brought the mouse to the platform ensuring it remained situated on the platform for a period of ten seconds. After eight days of escape latency testing, mice were subjected to a probe day wherein mice were placed in the pool for one trial without the platform in the pool.

On days 10 and 11, mice were subjected to reversal testing wherein the platform was now placed in the exact opposite quadrant during training (the front left zone). Escape latencies and swim paths were recorded with a video camera (Bosch, LTC0355/20; Pentax 3.5-8 mm lns, TS2V314BED) mounted directly above the pool. Data were recorded and analyzed by Ethovision v8 (v8.0.516) software. Analyses were performed using Prism 6.0a (Graph Pad Software).

2.9 Brain slice preparations and electrophysiology.

All manipulations were performed as we have previously described[89]. Briefly, uninjured adult male $Cx36^{-/-}$ and $Cx36^{+/+}$ mice and four weeks post KA seizure were collected. Mice were anaesthetized with halothane, cervically dislocated, decapitated and brains were removed. Hippocampal slices (300 μm thick) were cut with a Leica VT1000S vibratome. Hippocampal slices were kept in artificial cerebrospinal fluid (aCSF) at room temperature for one hour prior to recording. The aCSF contained 127 mM NaCl, 1.9 mM KCl, 1.2 mM KH_2PO_4, 2.4 mM $CaCl_2$, 1.3 mM $MgCl_2$, 26 mM $NaHCO_3$, 10 mM D-glucose, and equilibrated with 95% O_2-5% CO_2. During recording individual slices were contained in a custom built chamber between two grids continuously perfused with aCSF. The slice was illuminated from below so that it could be observed with a dissection microscope. Recordings were performed by whole cell clamping of CA1 neurons with Axopatch 1D amplifiers (MDS Analytical Technologies, Sunnyvale, CA, USA), using the blind version patch clamp technique[90]. Patch pipettes were made from pulled thin walled borosilicate glass. When filled with intracellular solution the patch pipettes had a resistance ranging from 2 to 8 MΩ. The intracellular solution was composed of 140.0 mM potassium gluconate, 10.0 mM Hepes, 10.0 mM KCl, 1.0 mM EGTA, 2.0 mM Na_2ATP, 1mg.ml^{-1} Lucifer Yellow (dipotassium salt). The solution was pH adjusted to 7.4 with KOH, and osmolarity adjusted to 310 $mOsmol^{-1}$ with sucrose. Neuronal input resistance and voltage-current relations were assessed by injecting rectangular-wave current pulses (±50-500 pA, 0.5 to 1s), then measuring the amplitude of the electronic potentials. Data were filtered between 2-5 kHz, and

digitized at 2-10 kHz (Digidata 1322, MDS Analytical Technologies), then stored using pCLAMP data acquisition software. Data analysis was accomplished using Clampfit 9 software (MDS Analytical Technologies).

To elicit glutamate release, brain slices were bathed in Mg-free aCSF containing 4-aminopyridine (4-AP) (Sigma, CA# 275875). To block NMDARs, 4-AP slices were exposed to D-(-)-2-Amino-5-phosphonopentanoic acid (D-AP5 or D-APV) (Tocris, CA# 0106). To block AMPARs, brain slices were then exposed to D-AP5 and 6-nitro-7-sulphamoylbenzo(f)-quinoxaline-2,3-dione (NBQX) (Tocris, CA# 0190). 4-AP was prepared in DMSO as a 100 mM solution. D-AP5 and NBQX were diluted first in ddH2O as a stock solution, and then diluted to required concentrations in aCSF immediately before use. The aCSF containing magnesium-free/4-AP was prepared without magnesium at a final concentration of 100 μM 4-AP. Drugs were applied to slices by perfusion from a line of 50 ml syringes with the main aCSF reservoir by a series of 3-way valves. The Magnesium-free/4-AP bathing medium was applied to slices for at least 20 minutes such that hippocampal neurons reached a steady-state spontaneous firing. The Ion channel blockers D-AP5, and subsequently NBQX were applied for a minimum of 10 minutes, saturating the bath at the desired concentration, and then recorded at steady-state for at least 20 minutes.

3. Chapter 3 – Results

3.1 Cx36 is developmentally regulated in the postnatal mouse hippocampus.

To profile changes in Cx36 mRNA and protein localization of Cx36 over the course of postnatal development, I used *in situ* hybridization (Fig. 3.1) and immunofluorescence (Fig. 3.2), comparing neonatal and adult mouse hippocampus. Robust mRNA expression was detected in the majority of hippocampal neurons in seven-day-old neonates (Fig. 3.1a-c). In two-month-old adult mice, Cx36 expression was restricted to a smaller subset of cells distributed throughout the granule layer of the dentate gyrus (GrDG) (Fig. 3.1d,e), pyramidal cell fields, *stratum oriens* (so), and *stratum lucidum* (slu) (Fig. 3.1d,f). No signal was detected in $Cx36^{-/-}$ neonates (data not shown) or adult hippocampus (Fig. 3.1g-i). By immunofluorescence, Cx36 puncta were detected in parvalbumin ($parv^{+}$) expressing inhibitory neurons of the hippocampus (Fig. 3.2a) and specifically in $parv^{+}$ neurons in the CA3a/b region of the adult hippocampus (Fig. 3.2b). Cx36 protein was found both at the cell body (Fig. 3.2b, i), and in processes (Fig. 3.2b, ii). We did not detect Cx36 protein in $parv^{+}$ cells in the hippocampus of $Cx36^{-/-}$ mice (Fig. 3.2c,d). Moreover, no immunoreactivity was detected throughout $Cx36^{-/-}$ brain sections confirming specificity of this antibody and lot (data not shown). We did not detect Cx36 in puncta at $PSD\text{-}95^{+}$ dendrites, $synapsin^{+}$ axons of pyramidal neurons or in $NeuN^{+}$ neurons in the CA fields beyond the $parv^{+}$ interneuron reactivity presented in Fig 3.2.

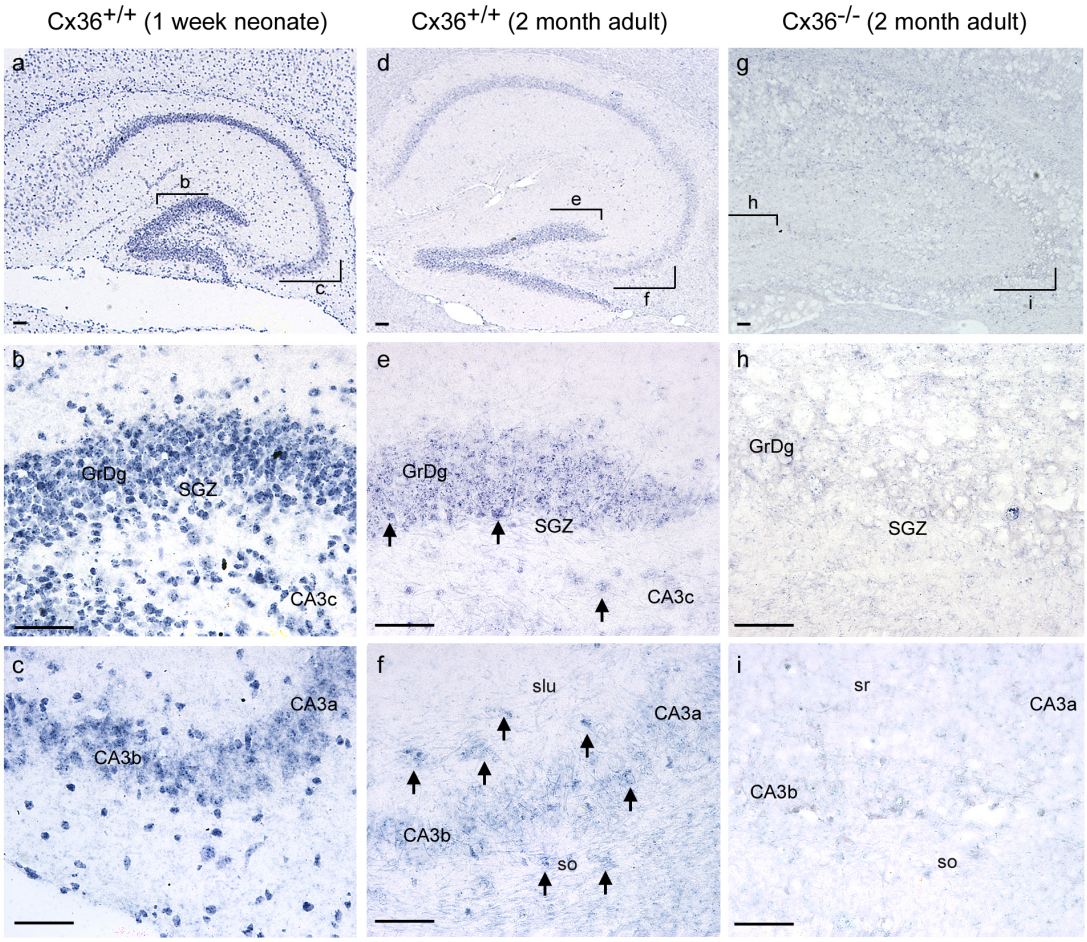
Cx36+/+ (1 week neonate)
Cx36+/+ (2 month adult)
Cx36-/- (2 month adult)
a
b
c
d
e
f
g
h
i
GrDg
SGZ
CA3c
CA3a
CA3b
slu
so
sr

Figure 3.1 Cx36 mRNA is expressed ubiquitously in neonatal hippocampus and is downregulated in the adult mouse.

Localization of Cx36 mRNA by *in situ* hybridization in the hippocampus of neonatal $Cx36^{+/+}$ (a-c), adult $Cx36^{+/+}$ (d-f), compared to adult $Cx36^{-/-}$ (g-i) mice. Low-magnification images of the hippocampus (a,d,g). Photomicrographs of the GrDg, subgranular cell layer (SGZ), and the *cornus amonis* 3c (CA3c) area of the pyramidal cell layer (b,e,h). Images of the CA3a/b region (c,f,i). Scale bars 50 μm. The location of higher magnification images in b,c,e,f,h,i are indicated in a,d,g.

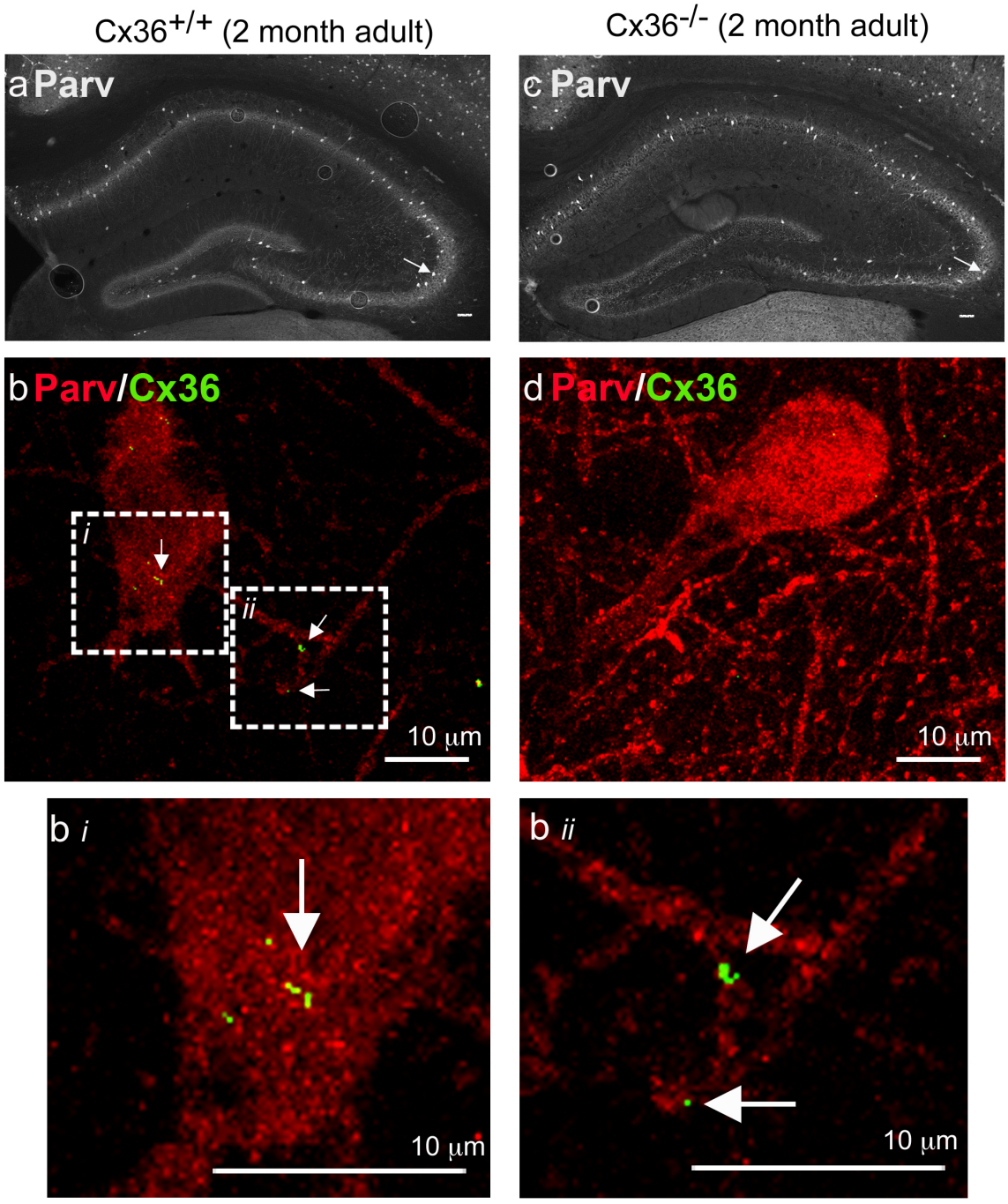
Cx36+/+ (2 month adult)
Cx36-/- (2 month adult)
a Parv
c Parv
b Parv/Cx36
d Parv/Cx36
i
ii
10 μm
10 μm
b i
b ii
10 μm
10 μm

Figure 3.2 Cx36 is detected at the cell soma and along neuritic extensions of parv+ interneurons in the hippocampal CA3a/b region.

Data from $parv^+$ immuno fluorescent labeling in adult $Cx36^{+/+}$ and $Cx36^{-/-}$ mice. Overall $parv^+$ labeling of the hippocampus in $Cx36^{+/+}$ and $Cx36^{-/-}$ mice (a,c). $Parv^+$ and Cx36 labeling of the CA3a/b region in $Cx36^{+/+}$ (b) and $Cx36^{-/-}$ (d) mice. Dotted boxes (insets) and arrows in b(i, ii) depict Cx36 protein expression at the $parv^+$ cell soma b(i) and along cell extensions b(ii). Scale bars (a,c) 50 μm, (b-d) 10 μm.

3.2 Loss of adult interneuronal Cx36-mediated GJIC enhances interictal burst frequency and increases the rate of seizure progression in adult mice.

To test whether developmental loss of Cx36 alters seizure behaviour *in vivo*, I performed a dose response of KA on $Cx36^{-/-}$ and congenic $Cx36^{+/+}$ mice. Mice (2.5 to 3 months of age) were injected intraperitoneally with 10-35 mg/kg KA. Seizure intensity was staged using the five-point behavioural scale we have described previously[83; 91]: Seizure stages include: 0, no response; 1, reduced locomotion and sedation; 2, automatisms including head bobbing, scratching, repetitive face washing, increased frequency of "freezing" and "wet-dog shakes"; 3, tremors and weak clonic convulsions; 4, intermittent followed by continuous rearing with forelimb clonus and loss of postural control; and 5, severe limbic seizures with respiratory difficulty resulting in mortality. Our laboratory has previously shown that mice must sustain stage 4 seizure for a minimum of 5 min to elicit significant pyramidal cell CA3a/b damage[92]. Thus, we can reproducibly control the extent of damage the seizures create to elicit the same lesion in every animal by limiting the duration of stage 4 seizure to 5 min using diazepam. This protocol, however, requires that all experimental animals exhibit the same seizure threshold (i.e., reach stage 4 seizure without progressing to stage 5 within this 5 min window using the same dose of KA).

I found that both $Cx36^{+/+}$ and $Cx36^{-/-}$ mice exhibited a very narrow dose-response window (Fig. 3.3a). In both genotypes, 15 mg/kg KA induced stage 4 seizure activity with low mortality rates in greater than 96% of all mice tested (Table 3.1). Seizure activity could be effectively limited in both genotypes after 5 min by injection with 5 mg/kg diazepam. Higher dosages (>15 mg/kg) caused both genotypes to progress rapidly to lethal stage 5 seizure (data not shown). At lower

dosages, $Cx36^{-/-}$ mice exhibited more rapid seizure induction than the wild-type mice. $Cx36^{-/-}$ mice injected with either 10 mg/kg or 15 mg/kg progressed through to stage 3 seizure faster than $Cx36^{+/+}$ controls (Fig 3.3a). Moreover, a higher percentage of $Cx36^{-/-}$ mice attained stage 4 seizure activity at lower dosages (i.e., 10 mg/kg) than $Cx36^{+/+}$ mice indicative of enhanced seizure susceptibility (Fig 3.3b). Taken together, these data demonstrate that $Cx36^{-/-}$ mice exhibit similar seizure thresholds as wild-type mice but progress more rapidly to stage 4 seizure.

To further test whether developmental loss of Cx36 alters seizure behaviour *in vitro*, we used the zero magnesium and 50 μM 4-AP (0 Mg^{2+}/4-AP) seizure model to generate spontaneous interictal-like activity in brain slice preparations (Fig. 3.4a-h). Whole-cell patch recordings from neurons in the CA1 were made to establish the extent of the Schaffer collateral glutamatergic input from the CA3a/b to the CA1.[1] Spontaneous interictal burst firing was higher in $Cx36^{-/-}$ slices compared to wild-type (Fig. 3.4a,b). Burst duration was comparable between genotypes (Fig. 3.4c). Perfusion with the NMDAR antagonist D-AP5 (40 μM) significantly increased burst rate in $Cx36^{+/+}$ slices without affecting $Cx36^{-/-}$ slice response (Fig. 3.4a, also compared b,d). Application of the AMPAR and kainate receptor antagonist NBQX to D-AP5-treated slices completely abolished interictal activity in both genotypes (Fig. 3.4a,e). Firing frequencies were restored in both genotypes following antagonist washout in 0 Mg^{2+}/4-AP (data not shown). These data are in agreement with the behavioural evidence that the loss of Cx36 increases seizure susceptibility both with

[1] These studies were performed in collaboration with Dr. David Spanswick. My role was to prepare the animals, assist in the acute slice preparation, observe the electrophysiology, assist in the analysis of the data, and interpret the results.

	Behavioural scale					
Genotype (Dosage)	**1**	**2**	**3**	**4**	**5 Mortality**	**Total number of mice**
WT (15 mg/kg)	0 (0%)	0 (0%)	3 (4%)	73 (96%)	0 (0%)	73
Cx36 $^{-/-}$ (15 mg/kg)	0 (0%)	0 (0%)	0 (0%)	50 (98%)	1 (2%)	51

Table 3.1 Sensitivity to KA induced seizures is comparable between $Cx36^{+/+}$ and $Cx36^{-/-}$ mice.

Seizure intensity was staged using a five-point behavioural scale. The optimal dosage was found to be 15 mg/kg triggering the stage 4 behavioural response in the majority of mice, with fewest reaching lethal stage 5 prior. Genotype had no effect on KA sensitivity.

respect to rate of seizure induction, sensitivity to KA, and interictal burst frequency.

In addition to interictal excitatory activity, 0 Mg^{2+}/4-AP also induced repetitive negative-going spontaneous inhibitory potentials (IPSPs) in CA1 neurons manifested during interictal interburst intervals (Fig. 3.4f). I found that the area but not frequency of CA1 IPSP activity was reduced in 0 Mg^{2+}/4-AP-treated $Cx36^{-/-}$ slices (Fig. 3.4g,h). Taken together, these data support previous reports that the loss of synchronous interneuron firing in $Cx36^{-/-}$ mice shapes pyramidal response to glutamatergic stimulation[19; 32; 93]; effects partially mimicked *in vitro* in wild-type slices by an overall reduction in burst frequency in 0 Mg^{2+}/4-AP, and subsequent burst firing frequency increase after D-AP5 application.

3.3 Enhanced seizure susceptibility is not due to alterations in glutamatergic receptor protein levels.

Alternatively, the loss of Cx36 over the course of postnatal development could alter the adult glutamatergic molecular machinery as suggested by recent reports that hippocampal NR2a/NR2b NMDAR ratios are elevated in the hippocampus of $Cx36^{-/-}$ mice[40]. To distinguish between these hypotheses, I assessed the molecular substrates of glutamatergic response in $Cx36^{-/-}$ and $Cx36^{+/+}$ hippocampus (Fig 3.5a,b; uninjured lanes). I did not detect any difference in the relative ratios of NMDAR subunits NR1, NR2A, and NR2B in the hippocampus between $Cx36^{+/+}$ or $Cx36^{-/-}$ mice (Fig 3.5a(i-iii),c; uninjured lanes). AMPAR subunits GluR1, and GluR2/3/4 also showed no difference between genotypes (Fig. 3.5b(i-iii); uninjured lanes). Postsynaptic density marker 95 (PSD95), flotillin (a lipid raft marker, data not shown), and Na^+K^+ATPase (a sodium/potassium channel marker) displayed no differences between genotypes (Fig. 3.5a(i-iii),b(i-iii); uninjured lanes).

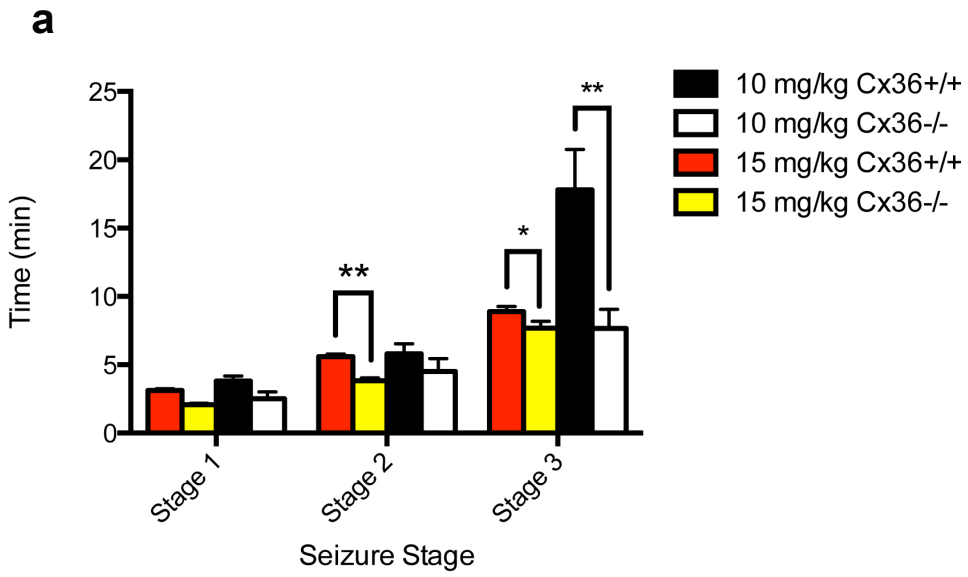
a
Time (min)
25
20
15
10
5
0
**
**
*
Stage 1
Stage 2
Stage 3
Seizure Stage
10 mg/kg Cx36+/+
10 mg/kg Cx36-/-
15 mg/kg Cx36+/+
15 mg/kg Cx36-/-

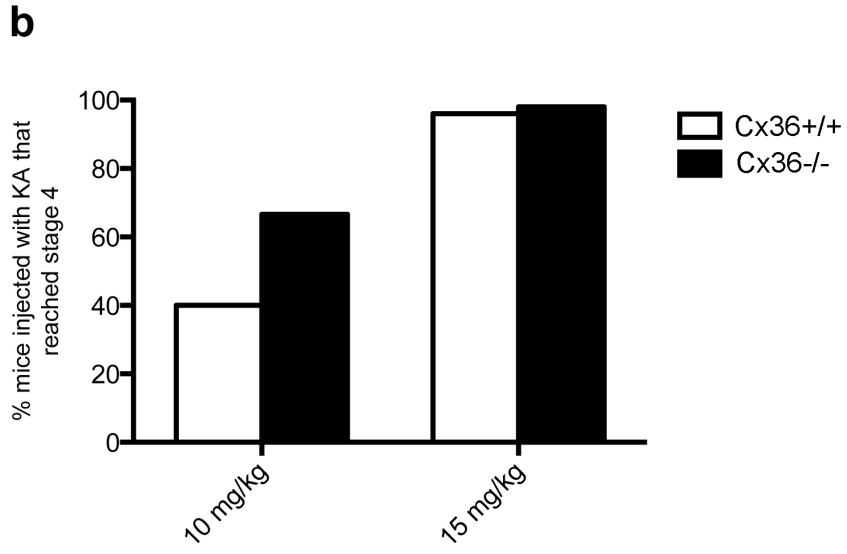
b
% mice injected with KA that reached stage 4
100
80
60
40
20
0
10 mg/kg
15 mg/kg
Cx36+/+
Cx36-/-

Figure 3.3 Seizure progression and susceptibility in adult $Cx36^{-/-}$ and $Cx36^{+/+}$ mice.

(a) Temporal kinetics of seizure progression in mice injected with 10 mg/kg and 15 mg/kg KA. (b) Percentage of mice that reached stage 4 seizure with 10 mg/kg and 15 mg/kg KA. Data represents the average time ± standard error of measurement (SEM) taken from mice to exhibit behavior characteristic of each seizure stage. Statistical analysis: Two-way Anova post hoc Holm Sidak's multiple comparisons: **P<0.005, *P<0.05. At 10 mg/kg n=5 for $Cx36^{+/+}$ and n=6 for $Cx36^{-/-}$ mice. At 15 mg/kg n=73 for $Cx36^{+/+}$ and n=51 for $Cx36^{-/-}$ mice.

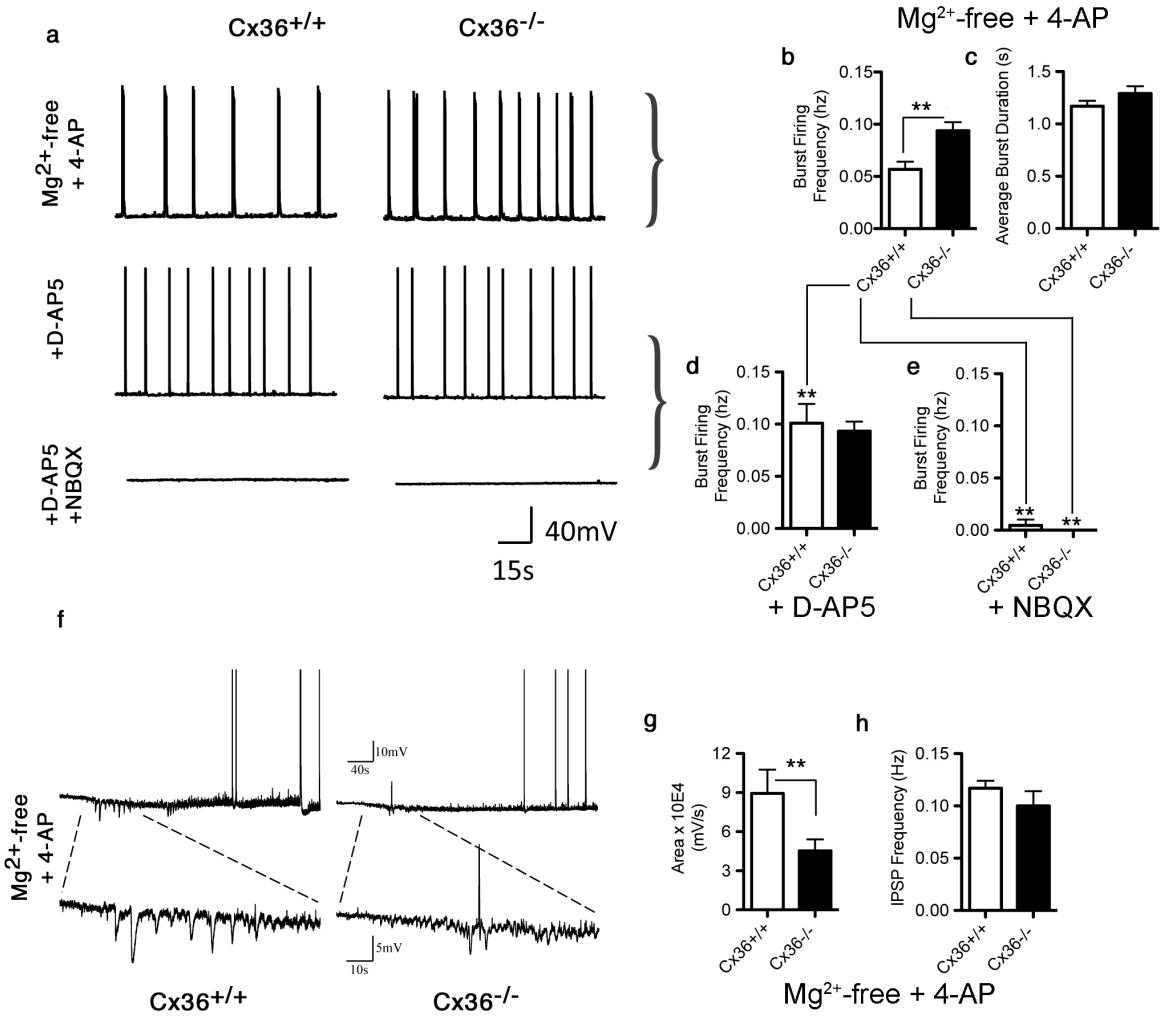
a
Cx36+/+
Cx36-/-
Mg2+-free + 4-AP
+D-AP5
+D-AP5 +NBQX
40mV
15s
Mg2+-free + 4-AP
b
Burst Firing Frequency (hz)
c
Average Burst Duration (s)
Cx36+/+
Cx36-/-
d
e
+ D-AP5
+ NBQX
f
10mV
40s
5mV
10s
Mg2+-free + 4-AP
Cx36+/+
Cx36-/-
g
Area x 10E4 (mV/s)
h
IPSP Frequency (Hz)
Mg2+-free + 4-AP

Figure 3.4 Interictal burst frequency is increased and the magnitude of repetitive negative-going spontaneous inhibitory potentials is decreased in $Cx36^{-/-}$ mice.

Data from brain slices of $Cx36^{+/+}$ and $Cx36^{-/-}$ mice are shown. Whole-cell patch recordings from neurons in the CA1 are depicted. (a) Representative traces of neuronal bursts in slices bathed with Mg^{2+} free 4-AP, +D-AP5, and + NBQX. (b,c) Statistical analysis of (b) burst firing frequency and (c) average burst duration in slices bathed with Mg^{2+} free 4-AP. Statistical analysis of burst firing frequency in slices bathed with (d) Mg^{2+} free 4-AP and D-AP5, and (e) +NBQX. (f) Representative traces of negative-going spontaneous burst activity (IPSPs) in slices bathed with Mg^{2+} free 4-AP. (g) Statistical analysis of area under the curve of IPSPs in slices bathed with Mg^{2+} free 4-AP. (h) Statistical analysis of IPSP frequency in slices bathed with Mg^{2+} free 4-AP. Statistics were Students t-test (b, g) or one way ANOVA (d, e, comparing all four conditions in b and d, or b and e as indicated by linking lines) with Tukey multiple comparisons post hoc tests. *$p<0.05$, **$p<0.001$. Data shown are mean ± SEM.

3.4 CA3a/b pyramidal neurons are protected from excitotoxic death in Cx36-/- mice.

To assess excitotoxic cell death in wild-type and Cx36$^{-/-}$ mice, seizures were induced by systemic administration of KA (15 mg/kg), and neuronal survival was compared in the CA3a/b at several time-points post-seizure. The viability of neurons in the CA3a/b was initially assessed by histological analysis of coronal sections though the hippocampus with hematoxylin and eosin (H&E) histology in parallel with immunofluorescence analysis of NeuN, a marker for newly born (terminally differentiated) and mature neurons (Fig. 3.6a-c). One week following seizure, there was a significant loss in the number of NeuN-positive cells in the CA3 in both wild-type and Cx36$^{-/-}$ mice (Fig. 3.6b,c), coinciding with tissue damage visualized by H&E staining in both genotypes (Fig. 3.6c). However, four-weeks following KA-induced seizure, NeuN labelling was restored to uninjured levels in Cx36$^{-/-}$ mice, but remained lower in wild-type mice. There was no significant change in the number of NeuN-labelled neurons in the DG at any time point post-seizure (data not shown).

While the loss of NeuN immunoreactivity in the CA3a/b might reflect neuron loss, brain injury characterized by metabolic perturbations, such as ischemia, has previously been reported to result in significant loss of NeuN antigenicity without actual neuronal cell loss[94]. To assess neuronal viability we used terminal deoxynucleotidyl transferase dUTP nick end labeling (TUNEL) to detect DNA fragmentation in dying cells (Fig. 3.7a,b). TUNEL analysis of the CA3 from Cx36$^{-/-}$ and wild-type mice following KA-seizure clearly demonstrates that Cx36 deletion almost completely protects cells from excitotoxic death (Fig. 3.7a,b). Wild-type mice exhibited significantly more TUNEL-labeling in the CA3 one week post-

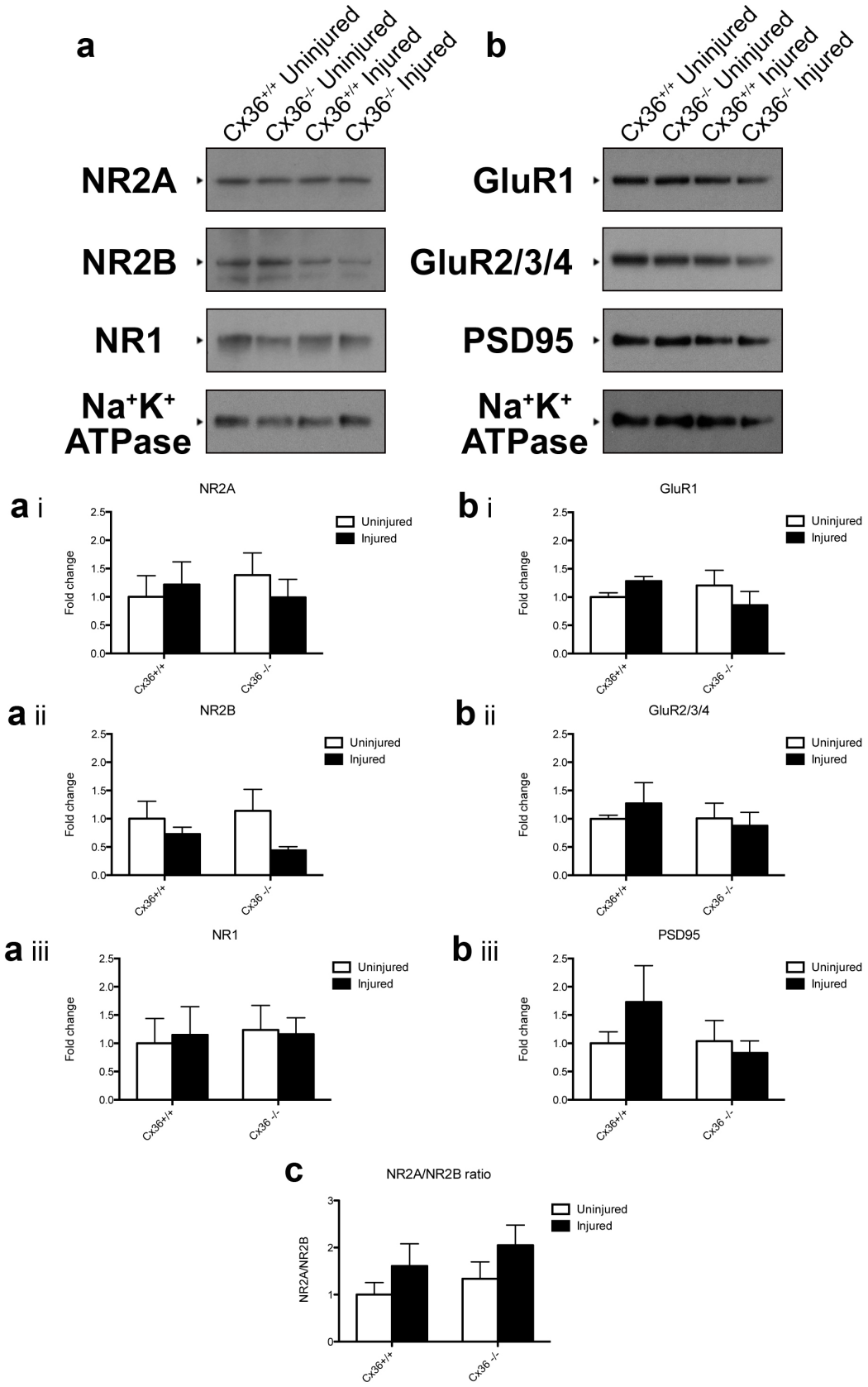
a
Cx36+/+ Uninjured
Cx36-/- Uninjured
Cx36+/+ Injured
Cx36-/- Injured
NR2A
NR2B
NR1
Na+K+ ATPase
b
Cx36+/+ Uninjured
Cx36-/- Uninjured
Cx36+/+ Injured
Cx36-/- Injured
GluR1
GluR2/3/4
PSD95
Na+K+ ATPase
a i
NR2A
b i
GluR1
a ii
NR2B
b ii
GluR2/3/4
a iii
NR1
b iii
PSD95
Uninjured
Injured
Fold change
Cx36+/+
Cx36 -/-
c
NR2A/NR2B ratio
NR2A/NR2B

Figure 3.5 Ionotropic glutamate receptor protein expression levels are comparable in uninjured mice and four weeks post KA-injury in both genotypes.

Ionotropic glutamate receptor expression was assessed at the protein level in hippocampal lysates prepared from uninjured mice and four weeks post KA-induced seizure. Representative immunoblots are shown (a-b). Quantitative densitometric analysis of NMDA and AMPA receptor blots (a,b) are presented (a(i-iii), b(i-iii)). Quantitative densitometric analysis of the NR2A/NR2B protein ratio is presented in (c). Protein levels were standardized to the Na^+K^+ATPase control band and normalized to the values in the uninjured $Cx36^{+/+}$ controls. Statistical analysis: Two way ANOVA, post hoc Holm Sidak (c). Each group contained n=3 mice. Data shown are mean ± SEM.

injury, while virtually no cells were labeled in the CA3 of $Cx36^{-/-}$ mice. No changes in NeuN or TUNEL labeling was observed in the DG in either group (data not shown).

3.5 In $Cx36^{+/+}$ mice a population of GABAergic interneurons are lost in the *stratum oriens* and CA3a/b regions of the hippocampus post KA-injury.

I further assessed survival of Cx36-expressing parv-positive interneurons in $Cx36^{+/+}$ and $Cx36^{-/-}$ mice following seizure. Cells were stereologically counted in the CA3a/b, CA3c, CA2, CA1, DG, hilus, *stratum lucidum*, *stratum radiatum*, and *stratum oriens* of the dorsal hippocampus (bregma -0.90 mm to bregma -2.40 mm) in uninjured mice and mice 28 days post KA seizure (Fig. 3.8a-e). Statistically reduced $Parv^{+}$ counts were observed in the CA3a/b, and *stratum oriens* of injured $Cx36^{+/+}$ mice compared to the uninjured $Cx36^{+/+}$ group (Fig. 3.8f, g). No significant difference was found in $Parv^{+}$ cell numbers of all other hippocampal regions counted between injury conditions (data not shown).

3.6 Cx36 mRNA and protein are downregulated 3.5 days and restored one-week after seizure localizing to a glial-like cell type.

To establish whether the kinetics of cell loss in $Cx36^{+/+}$ matched changes in Cx36 mRNA and protein expression, I used *in situ* hybridization and western blot analysis to assess mRNA and protein levels 0.5 and 1 week post KA-injury (Fig. 3.9a-g). In the DG, Cx36 mRNA was downregulated 3.5 days (0.5 wks) after seizure (Fig 3.9a,b) and cellular levels restored one-week post seizure (Fig 3.9a,c). Cellular localization was comparable in uninjured and one-week post seizure (Fig 3.9a,c). Kinetics were comparable in the CA3a/b layer but localization was markedly different (Fig 3.9d-f). Interestingly, mRNA expression was detected in a morphologically different, glial-like cell type in the CA3a/b region 7 days after seizure

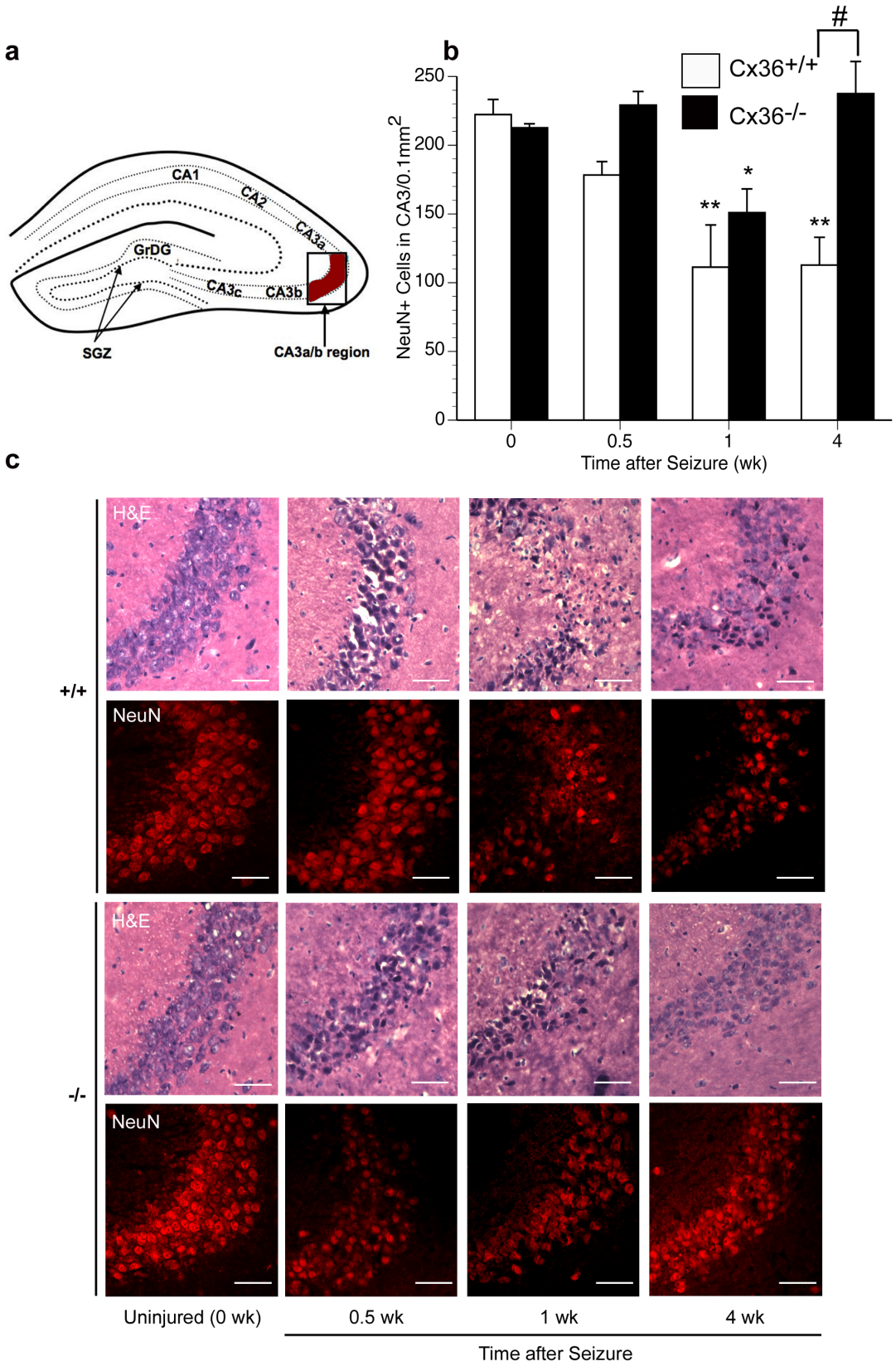
a
CA1
CA2
CA3a
GrDG
CA3c
CA3b
SGZ
CA3a/b region
b
Cx36+/+
Cx36-/-
#
*
**
**
NeuN+ Cells in CA3/0.1mm2
250
200
150
100
50
0
0
0.5
1
4
Time after Seizure (wk)
c
H&E
NeuN
+/+
-/-
Uninjured (0 wk)
0.5 wk
1 wk
4 wk
Time after Seizure

Figure 3.6 $NeuN^+$ cell counts are reduced one-week post injury in both genotypes and restored 4 weeks post injury only in $Cx36^{-/-}$ mice.

(a) Schematic highlighting the CA3a/b region of the hippocampus analyzed in (b-c). (b) $NeuN^+$ CA3a/b cell counts in uninjured, and 0.5, 1, and 4-week time points post KA-induced injury. (c) H&E staining and $NeuN^+$ images representing the CA3a/b region in $Cx36^{+/+}$ and $Cx36^{-/-}$ mice at the various post injury stages. Scale bars: 50 μm. Statistical analysis: Anova, post hoc Tukey: $^{**}p<0.01$, $^{*}p<0.05$ indicate statistically significant reduction in cell number relative to uninjured animals (0 wk). $\#p<0.05$. Asterisks indicate a statistically significant reduction between $Cx36^{+/+}$ and $Cx36^{-/-}$ mice at a given time point.

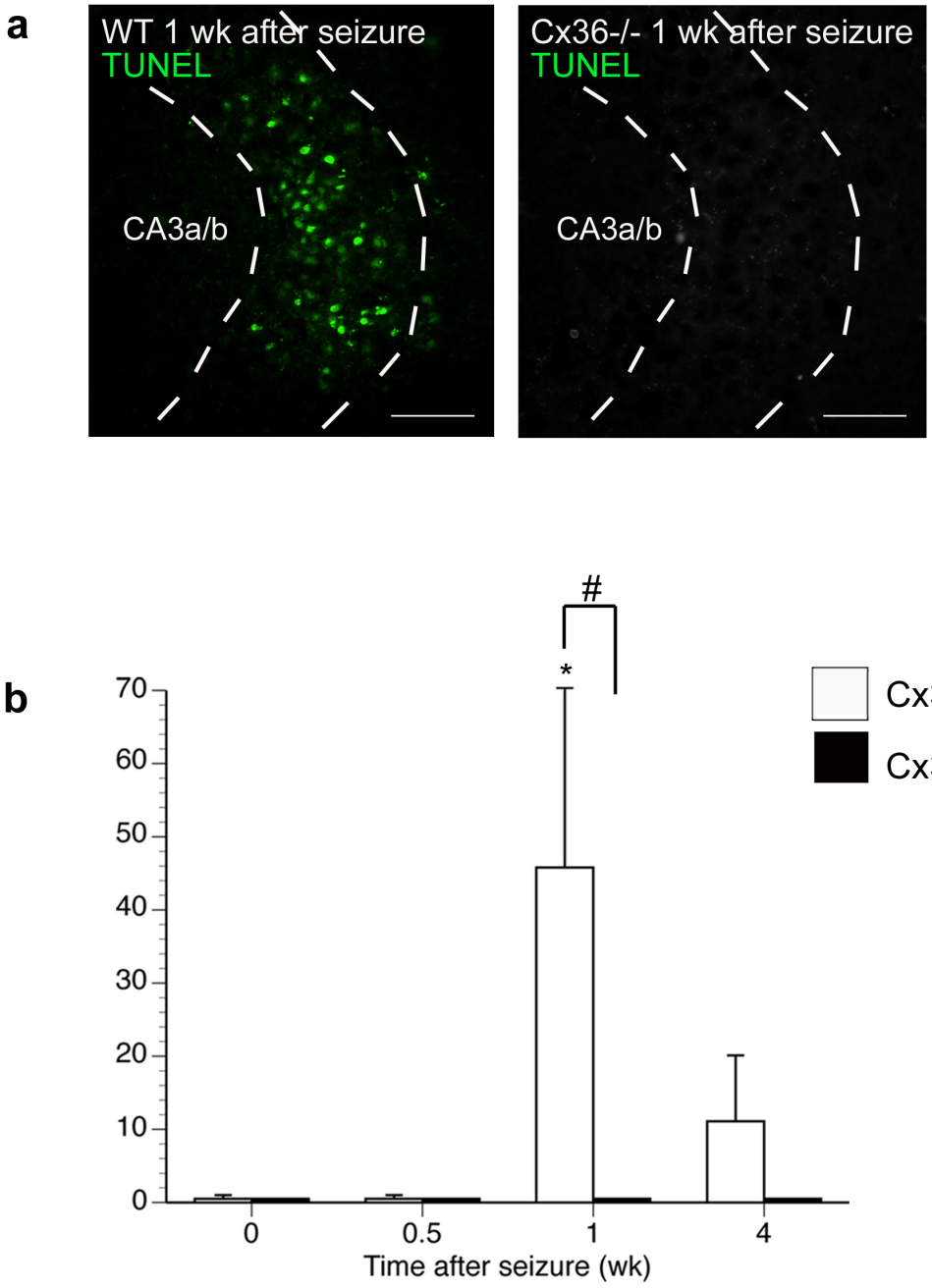
a
WT 1 wk after seizure
TUNEL
CA3a/b
Cx36-/- 1 wk after seizure
TUNEL
CA3a/b
b
#
*
Cx36+/+
Cx36-/-
70
60
50
40
30
20
10
0
0
0.5
1
4
Time after seizure (wk)

Figure 3.7 TUNEL^{+} cells are detected in CA3a/b cell one-week and four-weeks post injury in Cx36$^{+/+}$ but not Cx36-/- mice.

Quantification of TUNEL^{+} cell counts in the CA3a/b region of adult Cx36$^{+/+}$ and Cx36$^{-/-}$ mice over a time course post KA induced injury. (a) Image of the CA3a/b region in Cx36$^{+/+}$ and Cx36$^{-/-}$ mice one-week post injury. (b) TUNEL^{+} cell counts in the CA3a/b region of uninjured mice, and KA injured mice 0.5, 1, and 4 weeks post injury. Scale bars: 50 μm. Statistical analysis: ANOVA, post hoc Tukey: *$p<0.05$, #$p<0.05$. Asterisks indicate a statistically significant increase in TUNEL^{+} cells relative to uninjured animals (0 wk). # indicate a statistically significant difference between genotypes.

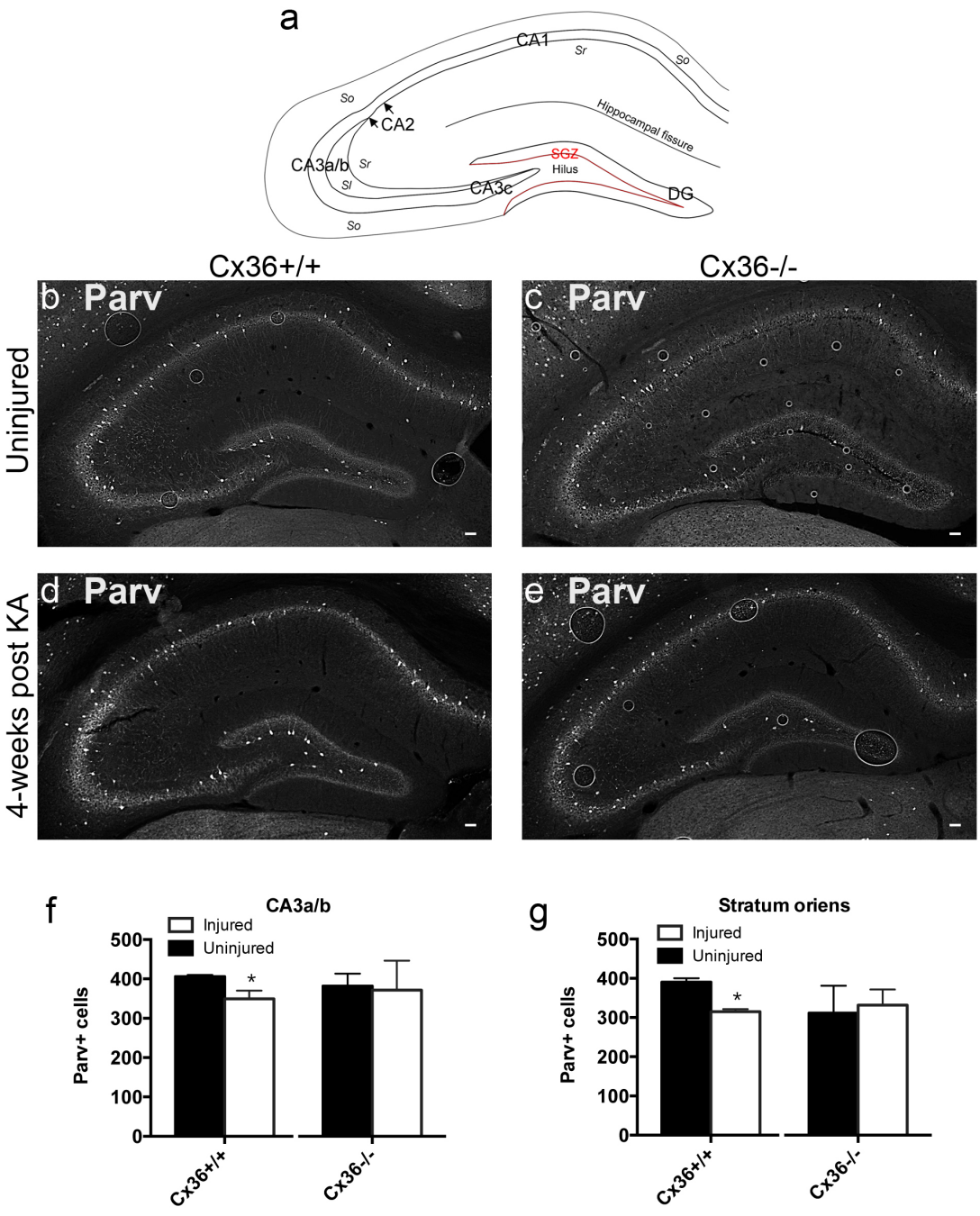
a
CA1
Sr
So
So
CA2
Hippocampal fissure
CA3a/b
Sr
Sl
SGZ
Hilus
CA3c
DG
So
Cx36+/+
Cx36-/-
Uninjured
4-weeks post KA
b Parv
c Parv
d Parv
e Parv
f
CA3a/b
Injured
Uninjured
Parv+ cells
500
400
300
200
100
0
*
Cx36+/+
Cx36-/-
g
Stratum oriens
Injured
Uninjured
Parv+ cells
500
400
300
200
100
0
*
Cx36+/+
Cx36-/-

Figure 3.8 Parv^{+} counts were reduced in the CA3a/b and *Stratum oriens* of injured Cx36$^{+/+}$ mice compared with the uninjured Cx36$^{+/+}$ group.

Data represents parv counts of Cx36$^{+/+}$ and Cx36$^{-/-}$ mice in various regions of the hippocampus in uninjured and four-weeks post injury. (a) Schematic indicating regions of the hippocampus quantified. (b-e) Representative images of parv labeling in Cx36$^{+/+}$ and Cx36$^{-/-}$ uninjured and brain sections of mice 4-weeks post KA-injury. Parv^{+} cell counts in (f) the CA3a/b region, and (g) the *stratum oriens*. (h) Parv^{+} cell counts representing all regions of the hippocampus, genotypes and injury conditions. Statistical analysis as follows: Mann-Whitney test, *$p<0.05$ (f, g). Scale bars 50 μm. n=3 mice per condition.

(Fig. 3.9f). These kinetics were confirmed at the protein level by immunoblotting (Fig 3.9g).

3.7 Cx36 is acutely and transiently expressed by activated microglia following kainate seizure.

The morphology of Cx36-positive cells detected by *in situ* hybridization in the CA3a/b (Fig 3.9a) suggested *de novo* expression by activated microglia. Microglia express the protein Iba1. To determine whether Cx36 is upregulated in activated microglia infiltrating degenerating CA3a/b neuronal fields, I looked at Cx36 and Iba1 expression in uninjured and injured tissue of $Cx36^{-/-}$ and $Cx36^{+/+}$ mice. In uninjured tissue, Cx36 protein expression was nearly devoid in Iba1-positive microglia (Fig. 3.10b). $Cx36^{-/-}$ mice served as a negative control to confirm antibody specificity (Fig. 3.10c). Seven days post KA-injury, a time where many $TUNEL^{+}$ cells were observed in the CA3a/b region of wild-type mice, I detected *de novo* protein expression of Cx36 in Iba1-positive cells (Fig. 3.10d, arrows). Notably, Cx36 protein expression was detected in cells in close proximity to larger neuronal-like nuclei (Fig. 3.10d yellow arrows represent Cx36 protein expression, and yellow arrowhead represents neuron-like nuclei). Further, Cx36 protein expression was found in Iba1 extensions surrounding nuclei consistent with the size of pyramidal cells (Fig. 3.10 inset d i, arrows represent Cx36 expression, arrowhead represents neuron-like nuclei). Cx36 expression was also found in Iba1 processes surrounding fragmented nuclei, indicative of a degenerated cell (Fig. 3.10d, orange arrows represent Cx36 protein expression in processes, and asterisk (*) indicate fragmented nuclei). Cx36-positive microglial processes were detected in distal processes (Fig. 3.10d,ii arrows). Iba1-positive cells were seen infiltrating the CA fields one-week post seizure in post-

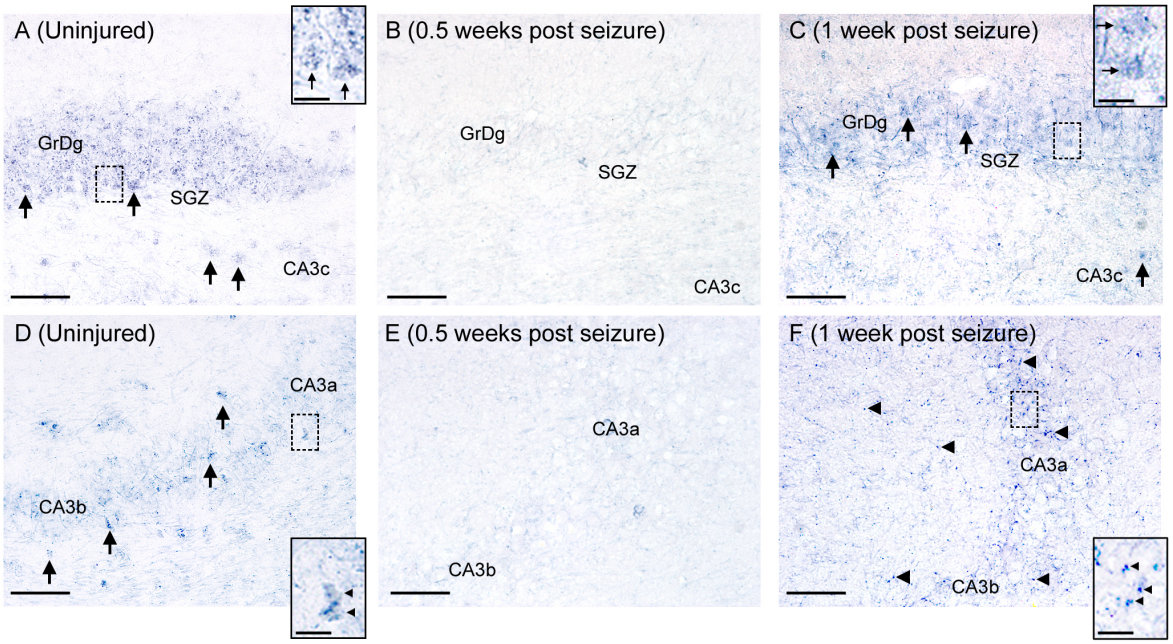
A (Uninjured)
GrDg
SGZ
CA3c
B (0.5 weeks post seizure)
GrDg
SGZ
CA3c
C (1 week post seizure)
GrDg
SGZ
CA3c
D (Uninjured)
CA3a
CA3b
E (0.5 weeks post seizure)
CA3a
CA3b
F (1 week post seizure)
CA3a
CA3b

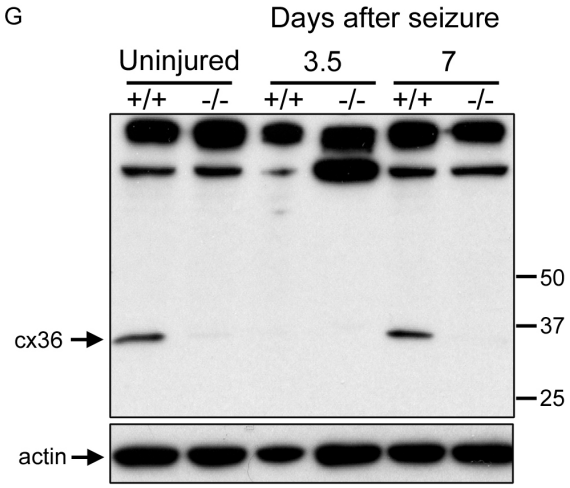
G
Days after seizure
Uninjured
3.5
7
+/+
-/-
+/+
-/-
+/+
-/-
50
37
25
cx36
actin

Figure 3.9 Cx36 expression is downregulated 0.5 weeks, and restored 1-week post injury; CA3a/b Cx36 mRNA appears to localize to glial cells following seizure.

Photomicrographs depict representative Cx36 mRNA expression detected by *in situ* hybridization in the GrDG (A-C) and the CA3a/b region (D-F). Protein levels assessed by Western blotting (G). Scale bars: 50 μm. Inset Scale bars: 10 μm.

seizure in both genotypes (data not shown). Four weeks after seizure, I found Cx36 localizing to remaining interneurons but not microglia in wild-type mice (data not shown).

3.8 Surviving neurons of the CA3 a/b region of the hippocampus in Cx36$^{-/-}$ mice are functional.

While these data provide converging evidence to indicate that CA pyramidal neurons and interneurons degenerate but do not die following KA-induced seizure in Cx36$^{-/-}$ mice, they do not assess functionality. To determine whether the surviving CA3 neurons in Cx36$^{-/-}$ mice are functional, I examined hippocampal circuit integrity, by evaluating burst activity in the CA1 as a measure of the Schaeffer collateral output of surviving cells in the CA3a/b to the CA1 (Fig. 3.11a,b)[95] and I compared behavioural indices of hippocampal learning and memory using the Morris Water maze (Fig. 3.12). For electrophysiology experiments, I used the same zero magnesium and 50 μM 4-AP (0 $Mg^{2+/}$4-AP) in a brain slice model to generate spontaneous interictal-like activity in hippocampal slices obtained from mice 4-weeks following seizure as described above (Fig 3.11a). As reported above, spontaneous interictal burst firing was lower in Cx36$^{+/+}$ slices compared to Cx36$^{-/-}$, but increased following NMDAR antagonism with D-AP5 in keeping with the inhibition of NMDAR-dependent repetitive spontaneous inhibitory potentials mediated by the synchronous input from Cx36-positive GABAergic interneurons on pyramidal neurons (Fig. 3.4a,b,d and Fig 3.11b,c,d). Four weeks following seizure, interictal burst frequency was elevated in Cx36$^{+/+}$ slices perfused with 50 μM 4-AP (0 $Mg^{2+/}$4-AP) (Fig 3.11c) consistent with the loss of interneurons in the Ca3a/b and *stratum oriens* (Fig 3.8f, g). There was no difference in Cx36$^{-/-}$ slices pre and post

seizure (Fig 3.11c). Following perfusion with D-AP5, burst frequency significantly decreased in $Cx36^{+/+}$ slices but not $Cx36^{-/-}$ (Fig 3.11c). Activity was completely abolished in all slices by further addition of NBQX and restored following washout of all antagonists (Fig. 3e, f). Taken together these data suggest that, in uninjured $Cx36^{+/+}$ animals, the non-NMDAR component of pyramidal cell glutamatergic activation is sufficient to maintain firing rate in face of NMDAR antagonism but that following kainate seizure this input is impaired, likely as a result of the loss of CA3a/b neurons. This deficit is not observed in $Cx36^{-/-}$ where neuronal loss is not detected. To establish whether these differences reflect the specific loss of CA3a/b neurons in $Cx36^{+/+}$ mice or a change in overall glutamate receptor expression, Western analysis was performed. No significant difference in NMDAR or GluR component was detected in whole hippocampal lysates nor were overall levels of pre and postsynaptic markers altered consistent with the specificity of this lesion to the CA3a/b (Fig 3.5). A more detailed look at the CA3a/b region of the hippocampus as opposed to the entire hippocampus may have proven more beneficial as this is where the neuronal loss is occurring in KA-treated wild-type animals.

To further address the functionality of protected CA3a/b neurons in $Cx36^{-/-}$ mice post excitotoxic injury, learning and memory was assessed behaviourally using the MWM test. There was a significant main effect of treatment on average escape latency per session ($F(3,36) = 5.433$ $p<0.01$ two way ANOVA) (Fig 3.12a). A post hoc Dunnett's multiple comparisons test showed that injured wild-type mice were significantly impaired, exhibiting higher escape latencies, compared to uninjured wild-type mice, but notably no significant difference was found between the uninjured wild-type and either the KA-injured $Cx36^{-/-}$ or uninjured $Cx36^{-/-}$ group.

There was a main effect of treatment on swim velocity ($F(3,36) = 6.954$ $p<0.01$ one way ANOVA) (Fig 3.12b). A Dunnett's post hoc comparison test showed significant differences between uninjured wild-type and injured wild-type groups ($p<0.001$) collapsed over the eight-day test period. Neither the performance of the uninjured $Cx36^{-/-}$ nor the injured $Cx36^{-/-}$ groups were statistically different from uninjured controls ($p>0.05$). There was no observed effect of treatment on distance moved ($F(3,36) = 0.979$ one way ANOVA) (Fig. 3.12b).

To further assess spatial learning and memory, after 9 days of testing the platform location was moved 180° and mice were required to use their previous memory of the spatial cues to adapt to the new position. During the reversal phase, injured $Cx36^{+/+}$ mice failed to adapt as effectively to the new platform location than uninjured $Cx36^{+/+}$, uninjured $Cx36^{-/-}$, or injured $Cx36^{-/-}$ mice on the second day of testing ($F(7,72) = 3.588$ $p<0.05$ one way ANOVA) (Fig 3.12a). Differences in behavioral performance between injured $Cx36^{+/+}$ mice and all other groups were likely due to their CA3a/b lesion and not motor deficits given that average swim distances were the same between all four groups, although swim speed was lower in the $Cx36^{+/+}$ injured cohort (($F(3,36) = 6.954$ $P<0.05$ one way ANOVA) (Fig. 3.12b). Together, these data provide converging electrophysiology and behavioural evidence that CA3a/b neurons are functionally protected from excitotoxic injury in $Cx36^{-/-}$ mice.

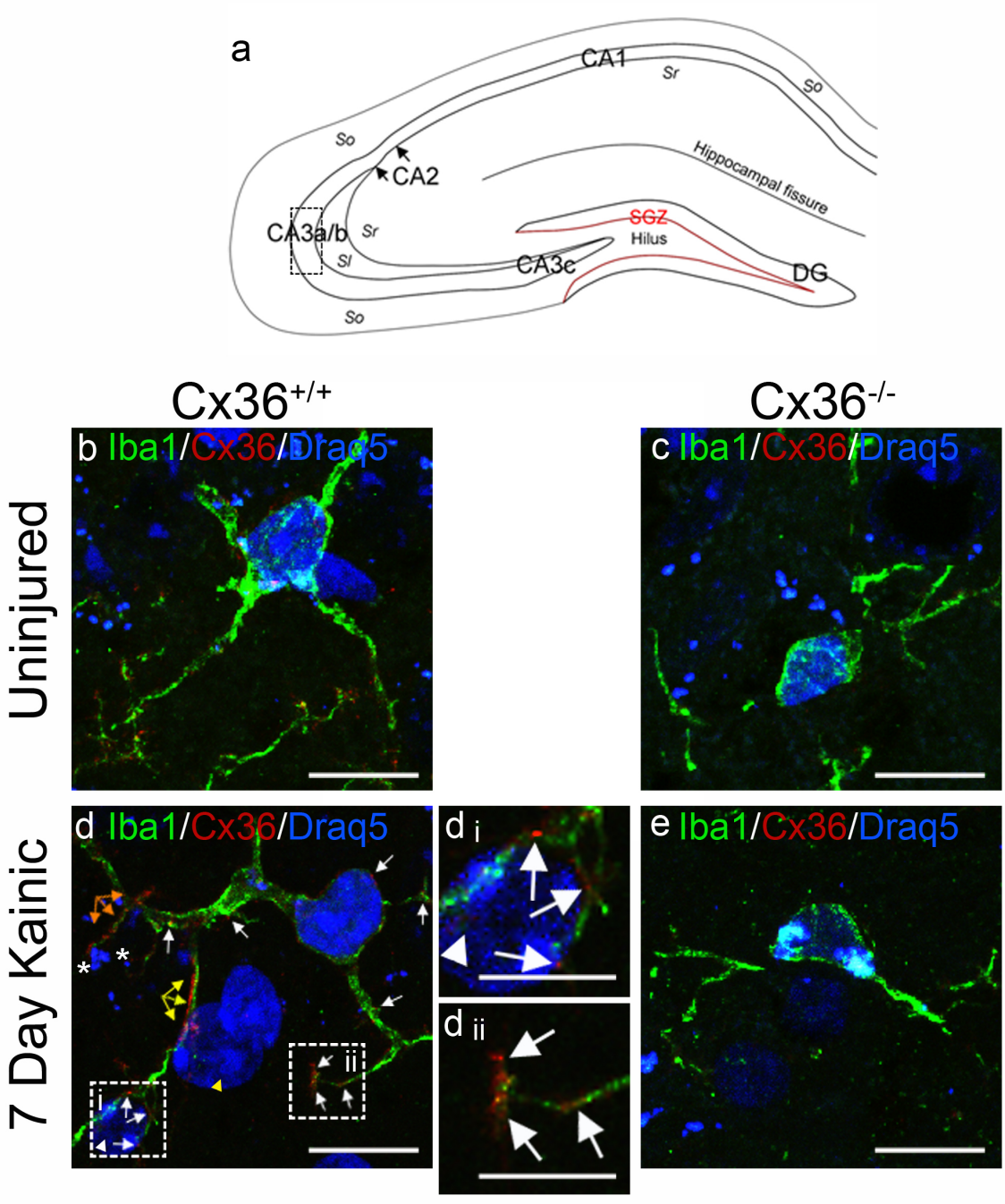
a
CA1
Sr
So
So
CA2
Hippocampal fissure
CA3a/b
Sr
Sl
SGZ
Hilus
CA3c
DG
So
Cx36+/+
Cx36-/-
Uninjured
7 Day Kainic
b Iba1/Cx36/Draq5
c Iba1/Cx36/Draq5
d Iba1/Cx36/Draq5
d i
d ii
e Iba1/Cx36/Draq5
i
ii
*
*

Figure 3.10 Dramatic upregulation of Cx36 protein expression is found in the CA3a/b region four weeks post KA-injury in $Cx36^{+/+}$ mice.

Double immunofluorescence labeling of Iba1 and Cx36. (a) Schematic of the hippocampus, specifically the CA3a/b region where the microglial images (b-e) were shot. (b) Cx36 protein labeling is nearly devoid in Iba1 expressing microglia in uninjured $Cx36^{+/+}$ mice. (c) Cx36 protein expression is absent in uninjured $Cx36^{-/-}$ mice. (d) *De novo* Cx36 protein expression is found in Iba1 expressing microglia in $Cx36^{+/+}$ mice one week post KA-injury. Arrows indicated Cx36 protein expression. Arrowheads indicate neuron-like nuclei. Asterisk (*) indicate fragmented nuclei. Inset (d i) represents Cx36 expressing Iba1 extensions (arrows) surrounding a neuron-like nuclei (arrowhead). Inset (d ii) represents a distal process of a Cx36 protein expressing Iba1 extension. (e) Cx36 protein is absent in $Cx36^{-/-}$ mice one-week post KA-injury. Scale bars: 10 μm. Inset Scale bars: 5 μm.

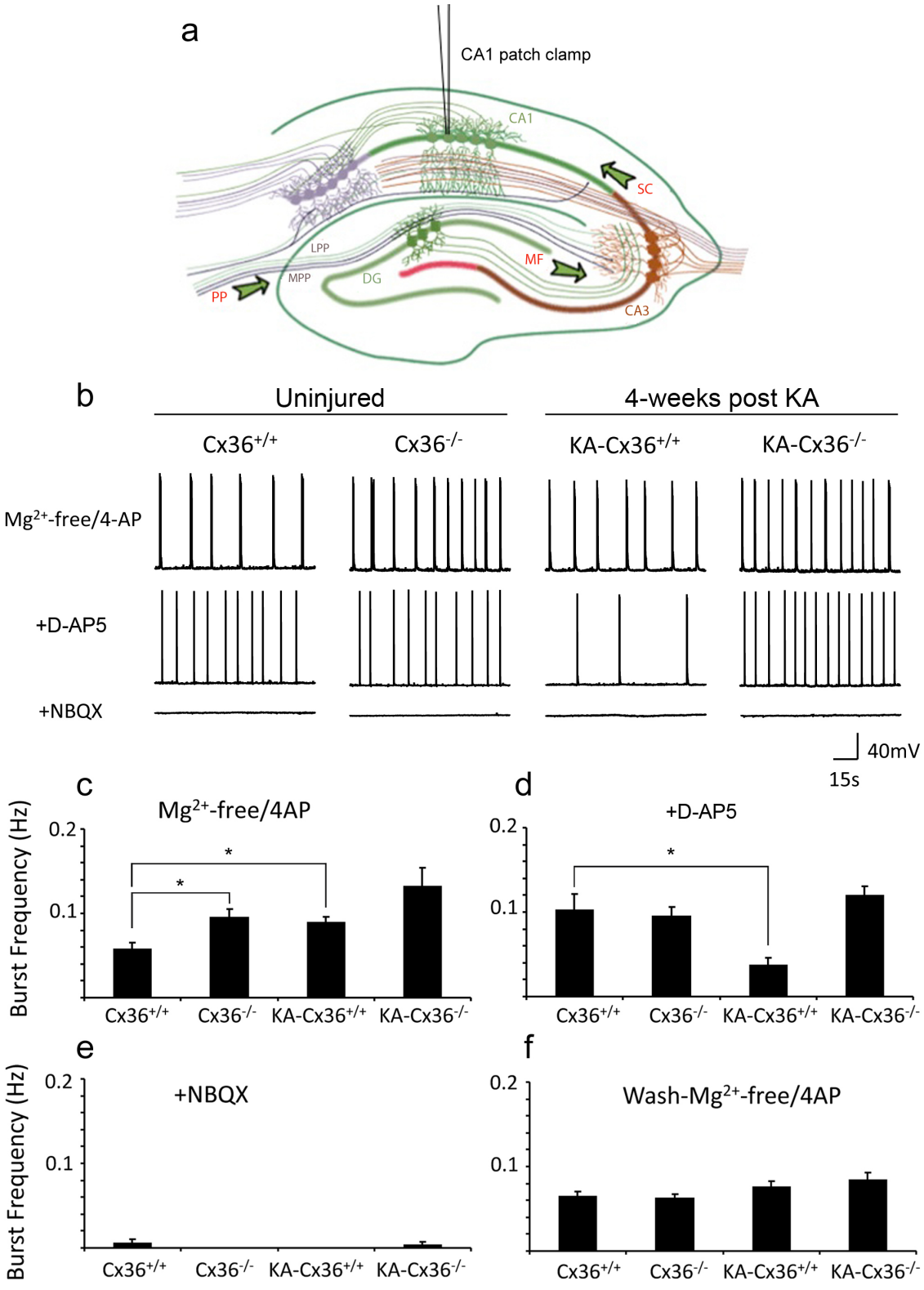
a
CA1 patch clamp
CA1
SC
LPP
MPP
DG
MF
PP
CA3
b
Uninjured
4-weeks post KA
Cx36+/+
Cx36-/-
KA-Cx36+/+
KA-Cx36-/-
Mg2+-free/4-AP
+D-AP5
+NBQX
40mV
15s
c
Mg2+-free/4AP
Burst Frequency (Hz)
0.2
0.1
*
*
Cx36+/+
Cx36-/-
KA-Cx36+/+
KA-Cx36-/-
d
+D-AP5
0.2
0.1
*
Cx36+/+
Cx36-/-
KA-Cx36+/+
KA-Cx36-/-
e
+NBQX
Burst Frequency (Hz)
0.2
0.1
Cx36+/+
Cx36-/-
KA-Cx36+/+
KA-Cx36-/-
f
Wash-Mg2+-free/4AP
0.2
0.1
Cx36+/+
Cx36-/-
KA-Cx36+/+
KA-Cx36-/-

Figure 3.11 Four weeks post injury $Cx36^{+/+}$ but not $Cx36^{-/-}$ mice exhibit impairments in glutamatergic input to the CA1.

Data represents electrophysiological trace recordings from brain slices obtained from $Cx36^{+/+}$ and $Cx36^{-/-}$ mice that were KA injured (4-weeks post) and uninjured. Neuron whole cell patch clamp recordings were done through the CA1 region to assess total functional output of the CA3a/b through the Schaeffer Collateral pathway. (a) Representation of patch clamp recording sites of CA1 neuron and functional pathways of the hippocampus (adapted from Aimone, et al 2006)[96]. (b) Representative trace recordings of pyramidal neurons in slice preps bathed in aCSF and Mg^{2+} free 4-AP, +D-AP5, and +NBQX. Burst firing frequency in slices bathed with (c) Mg^{2+} free 4-AP, (d) +D-AP5, (e) + NBQX, and (f) Mg^{2+} free 4-AP wash. Statistical Analysis: one way ANOVA, post hoc Tukey multiple comparisons test. *$p<0.05$. Data shown are mean ± SEM. Total numbers of neurons tested: n=14 uninjured $Cx36^{+/+}$, n=16 uninjured $Cx36^{-/-}$, n=16 KA-injured $Cx36^{+/+}$, n=14 KA-injured $Cx36^{-/-}$.

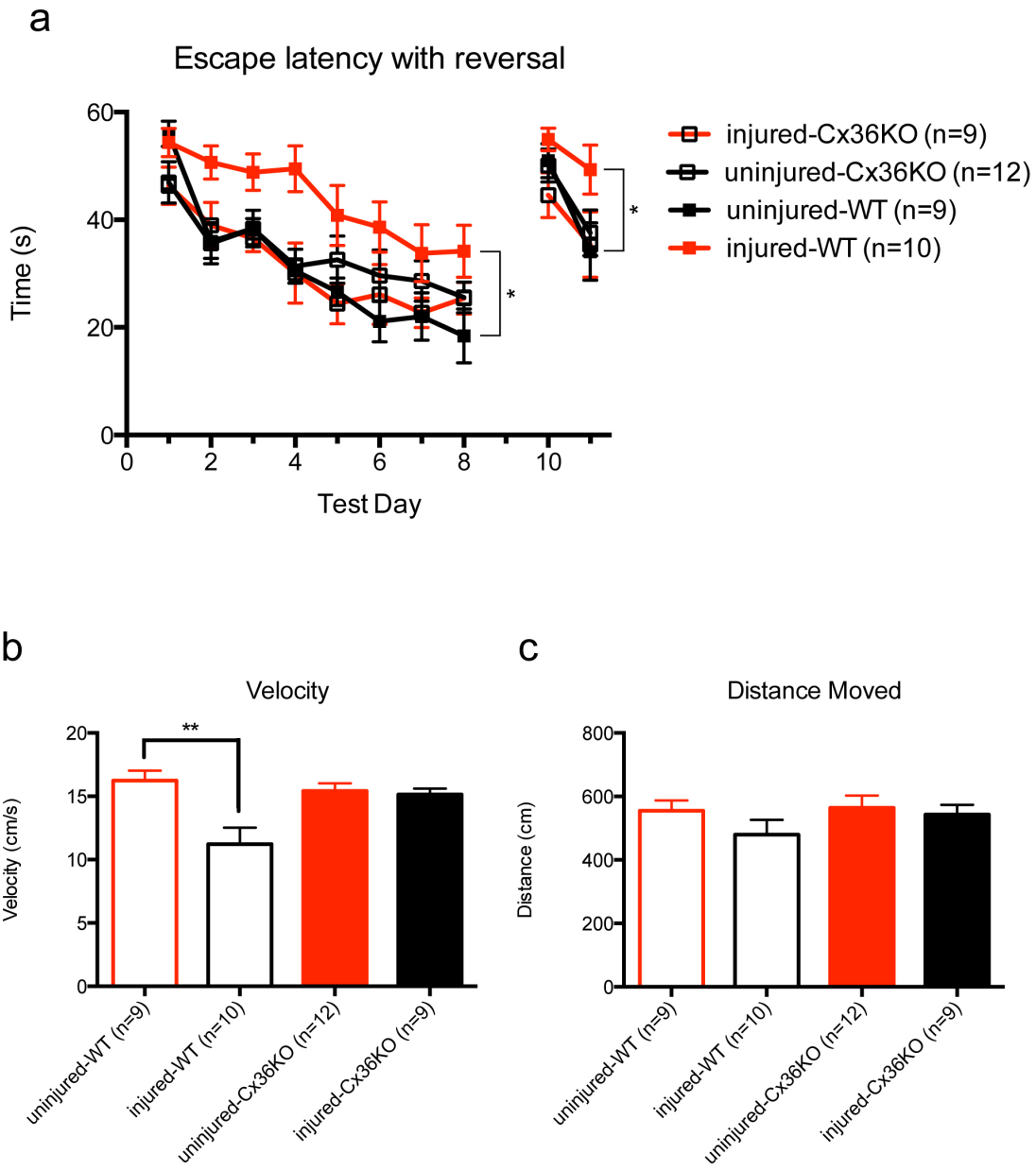
a
Escape latency with reversal
Time (s)
60
40
20
0
0
2
4
6
8
10
Test Day
*
*
injured-Cx36KO (n=9)
uninjured-Cx36KO (n=12)
uninjured-WT (n=9)
injured-WT (n=10)
b
Velocity
Velocity (cm/s)
20
15
10
5
0
**
uninjured-WT (n=9)
injured-WT (n=10)
uninjured-Cx36KO (n=12)
injured-Cx36KO (n=9)
c
Distance Moved
Distance (cm)
800
600
400
200
0
uninjured-WT (n=9)
injured-WT (n=10)
uninjured-Cx36KO (n=12)
injured-Cx36KO (n=9)

Figure 3.12 Behavioural impairment in learning and memory is only evident following KA-injury in $Cx36^{+/+}$ but not $Cx36^{-/-}$ mice.

Escape latency analysis of the MWM assessment of learning and memory. (a) Escape latency with reversal depicting all genotypes and injury conditions. (b) Velocity (cm/sec), and (c) distance moved (cm) over the first eight days of testing. Statistical analysis as follows; Escape latency, two way ANOVA, post hoc Dunnet's multiple comparisons test. Reverse escape latency, velocity, and distance moved, one way ANOVA, post hoc Dunnett's multiple comparisons test. **P<0.01, *P<0.05. Data shown are mean ± SEM.

4. Chapter 4 – Discussion

4.1 Summary.

In this thesis, I show that Cx36 is required for CA3a/b neuronal excitotoxic death in mice following KA-induced seizure. The data indicate that, following KA induced excitotoxic injury, focal CA3a/b hippocampal cell death occurs in the presence of Cx36, but in its absence this damage is abrogated. Surprisingly, death is not mediated by the opening of intrinsic Cx36 GJ or hemichannels in pyramidal neurons. Cx36 protein was not detected pre- or post-injury in pyramidal cells, but localized to parv^{+} interneurons in uninjured mice and activated microglia in injured mice. Moreover, one-week post seizure, when TUNEL-reactivity in CA3a/b neurons, is maximal, Cx36 expression in microglia is dramatically upregulated. Further, these Cx36 expressing microglia are found in close proximity to, and in close contact with non-Iba1 expressing cells with neuron-like morphology. Cx36 expressing microglial extensions are found surrounding these non-Iba1 expressing neuron-like cells. In the absence of Cx36, neuronal survival is enhanced in the CA3a/b region of Cx36$^{-/-}$ mice 4-weeks post KA-injury and surviving neurons are functional as determined by electrophysiological and behavioural assessment. Taken together, these data suggest a novel neuron-glial nexus important for completion of a delayed neuronal death program *in vivo*.

4.2 Connexin-mediated microglia-neuronal interactions represents a novel cell death mechanism underlying excitotoxicity.

The finding that the absence of Cx36 is neuroprotective in excitotoxic conditions is consistent with previous reports that, under conditions of NMDAR

hyperfunction, neurons are protected when they do not express Cx36[48]. Further, during excitotoxic conditions created due to ischemia, mice with Cx36 null mutation were shown to have significantly reduced cortical infarct volume[31; 97]. However, these authors postulated that Cx36-dependent ischemic cell death was due to the "bystander effect," or cortical spreading depolarization, through Cx36 gap junctions between target neurons. These cortical observations post ischemia, do not account for the fact that Cx36 expression has only been observed in interneurons, at least in the hippocampus, and not throughout all neuronal cell types which are dying during ischemic conditions[3; 19; 98]. Wang *et al.* 2012 postulates that observed elevations of Cx36 expression 2 hours post ischemia increases GJ coupling through the cortex leading to the spread of ischemia mediated neuronal death[31]. This study, however, does not show cell pyramidal cell type expression of Cx36 pre or post injury.

Here, I show that despite the lack of Cx36 expression, in target cells, the loss of pyramidal neurons, likely those expressing AMPAR/KAR in the CA3a/b region is abrogated by Cx36 null-mutation. In the murine hippocampus Cx36 has classically been shown in inhibitory interneurons[3; 19]. There are recent reports suggesting that, in the rat, Cx36 is expressed in pyramidal cells[29; 30]. However, by both *in situ* hybridization and immunofluorescence, I show that expression of Cx36 is undetectable, or below the level of detection in pyramidal neurons and shifts from GABAergic interneurons of the CA3a/b in uninjured mice to activated microglia post KA-induced excitotoxicity. These localization data are supported by electrophysiological assessment wherein the $Cx36^{-/-}$ phenotype is consistent with a loss of synchronous interneuron firing shaping pyramidal response to glutamatergic stimulation recapitulated *in vitro* in wild-type slices by an overall reduction in 4-AP-

induced interneuron activation after D-AP5 application, and following injury by the loss in Cx36 interneurons. Together, these data suggest that observed CA3a/b cell death is not through the "bystander effect" wherein dying pyramidal neurons pass toxic second messengers to coupled pyramidal neurons but rather through *de novo* expression of Cx36 in microglia, and a microglia-neuron interaction.

4.3 Mechanism of neuronal death in KA-injured Cx36$^{+/+}$ mice.

The observed expression of Cx36 in microglia *in vivo* is consistent with previous reports *in vitro*[63]. I postulate that *de novo* expression of Cx36 in activated microglia during excitotoxic CA3a/b injury is forming GJIC with interneurons through a Cx36-Cx36 homotypic channel, and with pyramidal neurons through a Cx36-Cx45 heterotypic GJ[25; 99]. Previous studies in the mouse have reported that pyramidal cells express Cx45[16], and Cx36 and Cx45 can form compatible heterotypic channels[25]. Microglia-neuron GJIC have previously been reported *in vitro*, and microglia have reportedly formed GJIC with neurons in co-cultures[63]. It is possible, even likely, that activated microglia can release death signals to neurons through GJs such as Ca^{2+}, NO, superoxide radical, prostanoids, and cytokines, initiating cell death pathways, such as mitochondrial dysfunction, cytochrome c release initiating the apoptosome complex, leading to caspase 3 activation creating nuclear condensation and subsequent apoptosis, or activating necrotic cell death pathways such as lipid peroxidation causing damage to the cell membrane as described in Wang et al. 2005[51; 63; 74]. Eichhoff *et al* 2011, demonstrated that activated microglia were found to locate and kill damaged neurons through the release of intracellular Ca^{2+} stores, signaling focal destruction of the damaged cells in their vicinity[74]. They

further report that microglia do not become activated under normal physiological conditions, or conditions of strong neuronal activity, rather they become activated only in times of neuronal damage[74]. It is possible that microglia Ca^{2+} signaling is highly sensitive and specific for the identification of damage in the microglial environment through Cx36, and subsequently destroys these damaged cells through Ca^{2+} delivery through Cx36-Cx45 GJ in pyramidal cells, or Cx36-Cx36 in interneurons (Fig. 4.1a).

Alternatively, in KA-injured $Cx36^{+/+}$ mice, activated microglia in the CA3a/b region could be releasing Ca^{2+} into the extracellular space through Cx36 hemichannels. The hemichannel of death hypothesis is supported by evidence that Cx36 can form functional single membrane channels in non-junctional membranes[21]. Activated microglial have been implicated in causing neuronal death *in vitro* through the release of toxic factors though hemichannels[44]. Thus, another possible mechanism of observed neuronal cell death is that activated microglia are recruited to the injured CA3a/b hippocampal area and are releasing Ca^{2+} into the extracellular space. Excess Ca^{2+} can be taken up by neurons through voltage gated calcium channels, pannexin1 channels, activated NMDARs, Cx45 hemichannels (pyramidal cells), and/or Cx36 hemichannels (interneurons) (Fig. 4.1b).

4.4 Mechanism of neuronal survival in KA-injured $Cx36^{-/-}$ mice.

It is further possible, that, in KA-injured $Cx36^{-/-}$ mice, microglia are providing neurotrophic support to CA3a/b neurons. In the absence of Cx36, microglia may not become activated post KA-injury as they do in injured wild-type mice. Here, I qualitatively observed the same degree of microglial infiltration in the CA3a/b zone

1-week following seizure, however morphology (activated or resting) has yet to be assessed. Ramified microglia have previously been reported, under excitotoxic conditions, to aid in neuronal survival by release of neurotrophins[64]. Hence, it is possible that in the absence of frank microglial activation neurons in KA-injured $Cx36^{-/-}$ mice are rescued.

4.5 Surviving neurons in KA-injured Cx36-/- mice are functional.

Finally, the discovery that the absence Cx36 prevents functional KA-induced excitotoxic damage is indeed an exciting one. Here, converging electrophysiological and behavioural measures confirm compelling functional protection. Pyramidal neurons, and interneurons of the CA3a/b express AMPAR/KARs[56], and are lost in the CA3a/b region of the hippocampous post KA-injury[56; 100; 101]. In fact, pyramidal neurons are known to express highest levels of the KAR subunit GluR6, which is highly sensitive to KA[56; 102]. In support of selective neuronal loss, I found that an AMPAR/KAR component is lost post KA-injury through electrophysiological assessment. The loss of a CA3a/b AMPAR component is consistent with structural synaptic reorganization following neuronal loss[56]. AMPAR are important in learning and memory[103]. The loss of an AMPAR component speaks to a functional loss in $Cx36^{+/+}$ mice, and the fact that this component is not lost in injured $Cx36^{-/-}$ mice highlights the functionality of the CA3a/b region post injury.

These findings are supported by, and help to explain the deficit in learning and memory observed in MWM in injured $Cx36^{+/+}$ mice. It is important to note that the impaired escape latency in $Cx36^{+/+}$ mice is not due to motoric impairment. The KA-injured cohort of wild-type mice did exhibit a significantly lower swimming

velocity than the uninjured wild-type group of animals, yet were still capable of traversing the same distance as uninjured $Cx36^{+/+}$ and $Cx36^{-/-}$ mice. KARs, have only been reported in neuromuscular junctions of invertebrates, and not mammals, thus peripheral CNS impairment is likely not the cause of the deficits observed in injured wild-type animals in the MWM[104; 105]. More exciting is the finding that injured $Cx36^{-/-}$ mice are behaviorally comparable to uninjured animals thus neurons are functionally spared. Taken together, theses findings potentially identify Cx36 as a therapeutic target for excitotoxic conditions.

4.6 Significance of research: A therapeutic target for excitotoxic conditions.

Ultimately, in this thesis, I have shown that Cx36 plays a primary role in transducing KA-induced excitotoxic damage in mice, and that toxicity is likely due to connexin-mediated neuronal-glial interactions dependent on microglial Cx36 expression and not on intrinsic Cx36 expression by pyramidal neurons. This provides a novel and therapeutically targetable mechanism for excitotoxic damage.

With limited therapeutics available in excitotoxic diseases such as temporal lobe epilepsy (TLE), it is very important to discover new drug therapies. Approximately 35% of patients with TLE are resistant to antiepileptic drugs (AED)[106]. In severe conditions patients require hippocampal resection surgery[106]. Other therapies when AEDs are not effective include vagus nerve stimulation (VAS), which can half seizure instances in one third of patients[107]. Cell replacement therapies are in preliminary phases and still require much study in animal models before they can be tested clinically. These are examples of treatments when AEDs are not possible. Current AEDs treat the occurrences of seizure thereby attempting to limit the

severity of seizure during occurrences. These drugs include sodium channel blockers, calcium channel blockers, GABA receptor agonists, GABA transaminase inhibitors, GABA reuptake inhibitors, glutamic acid decarboxylase (GAD) enhancers, potassium channel openers, glutamate blockers, and carbonic anhydrase inhibitors[108]. Now with the development of third generation, or novel AEDs, potentially more beneficial treatments are being discovered[109]. However, more studies are required to see if new antiepileptic drugs are able to effectively manage refractory, or drug resistant forms of epilepsy[109]. Current drugs that are effective in managing the occurrences, or severity of seizure in epilepsy, are also beneficial in treating other excitotoxic related disease conditions such as migraines (related to seizure), PD, AD, and ischemia[109; 110; 111]. It remains clear that new drugs need to be discovered through animal models and screening methods in order to progress the advancement of patient well being and the human condition[54; 109]. Currently antiepileptic drug treatments are not fully known to be neuroprotective in excitotoxic seizure conditions[112]. To date there are no drugs on the market that can protect neurons from cell death post excitotoxic injury in the epileptic condition, or prevent the generation of ectopic hyperexcitable circuitry causing recurrent seizures[113; 114]. Therefore, this study highlights Cx36 as a novel target for seizure induced excitotoxicity, and can possibly be applied to other models of excitotoxicity.

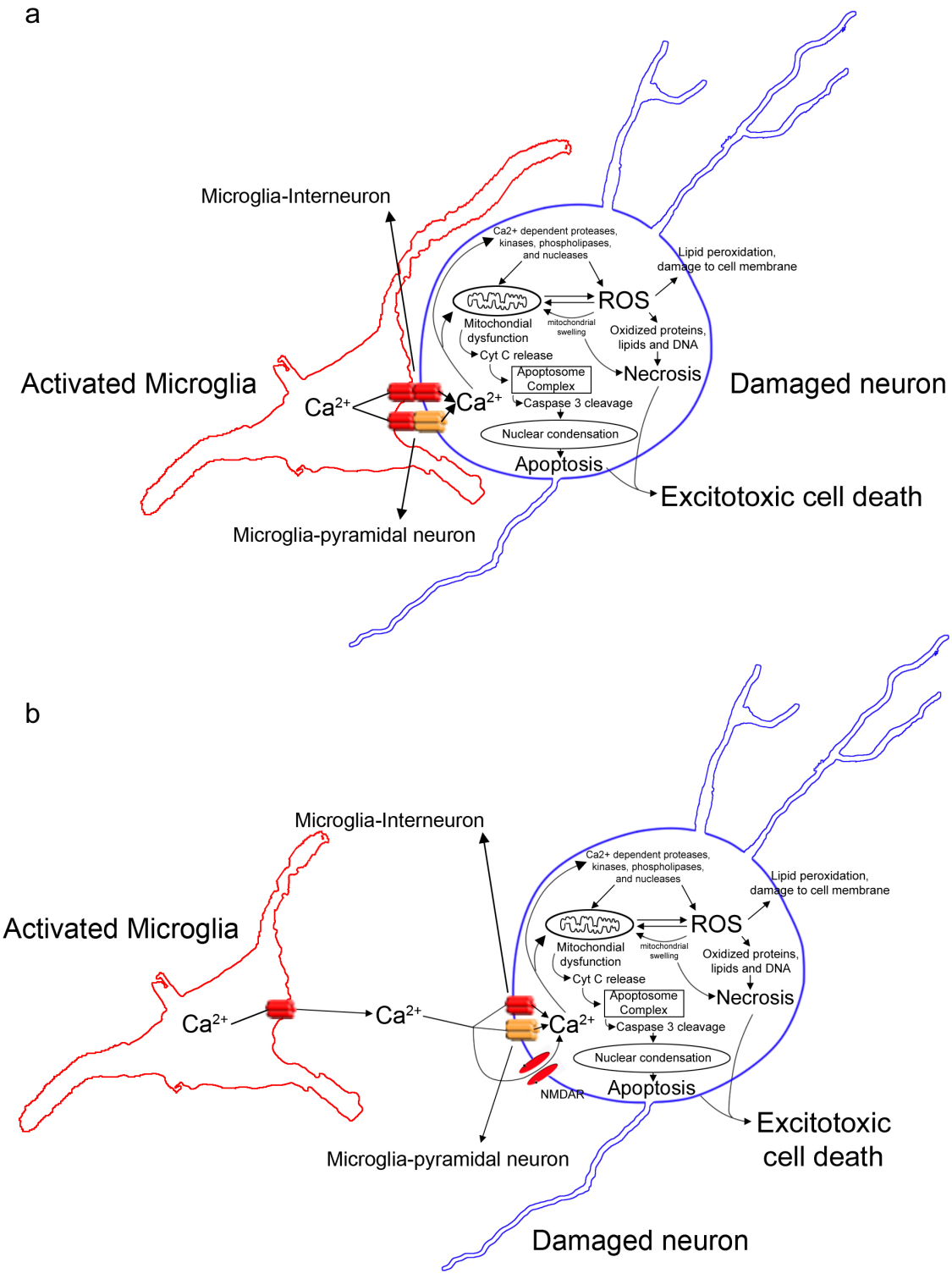
a
Microglia-Interneuron
Activated Microglia
Damaged neuron
Microglia-pyramidal neuron
Ca2+ dependent proteases, kinases, phospholipases, and nucleases
Lipid peroxidation, damage to cell membrane
ROS
Mitochondial dysfunction
mitochondrial swelling
Oxidized proteins, lipids and DNA
Cyt C release
Apoptosome Complex
Necrosis
Caspase 3 cleavage
Nuclear condensation
Apoptosis
Excitotoxic cell death
Ca2+
Ca2+
b
Microglia-Interneuron
Activated Microglia
Ca2+
Ca2+
Ca2+
NMDAR
Microglia-pyramidal neuron
Ca2+ dependent proteases, kinases, phospholipases, and nucleases
Lipid peroxidation, damage to cell membrane
ROS
Mitochondial dysfunction
mitochondrial swelling
Oxidized proteins, lipids and DNA
Cyt C release
Apoptosome Complex
Necrosis
Caspase 3 cleavage
Nuclear condensation
Apoptosis
Excitotoxic cell death
Damaged neuron

Figure 4.1 Mechanisms of microglial induced neuronal death.

Mechanism of observed neuronal death in $Cx36^{+/+}$ mice post KA-injury in the CA3a/b region of the hippocampus. (a) Through a Cx36 involving microglia-neuron GJ interaction initiating cell death pathways; Cx36-Cx45 microglia-pyramidal cell GJ, and Cx36-Cx36 microglia-interneuron GJ. (b) Through hemichannel activation in Cx36 expressing microglia, releasing death factors and initiating cell death pathways in damaged neurons.

References

1. Milks, L. C., Kumar, N. M., Houghten, R., Unwin, N. & Gilula, N. B. (1988). Topology of the 32-kd liver gap junction protein determined by site-directed antibody localizations. *EMBO J* **7**, 2967-75.
2. Yeager, M. & Gilula, N. B. (1992). Membrane topology and quaternary structure of cardiac gap junction ion channels. *J Mol Biol* **223**, 929-48.
3. Sohl, G., Maxeiner, S. & Willecke, K. (2005). Expression and functions of neuronal gap junctions. *Nat Rev Neurosci* **6**, 191-200.
4. Naus, C. C. & Bani-Yaghoub, M. (1998). Gap junctional communication in the developing central nervous system. *Cell Biol Int* **22**, 751-63.
5. Kamermans, M., Fahrenfort, I., Schultz, K., Janssen-Bienhold, U., Sjoerdsma, T. & Weiler, R. (2001). Hemichannel-mediated inhibition in the outer retina. *Science* **292**, 1178-80.
6. Goodenough, D. A. & Paul, D. L. (2003). Beyond the gap: functions of unpaired connexon channels. *Nat Rev Mol Cell Biol* **4**, 285-94.
7. Kumar, N. M. & Gilula, N. B. (1996). The gap junction communication channel. *Cell* **84**, 381-8.
8. Mroue, R. M., El-Sabban, M. E. & Talhouk, R. S. (2011). Connexins and the gap in context. *Integr Biol (Camb)* **3**, 255-66.
9. Xu, X., Francis, R., Wei, C. J., Linask, K. L. & Lo, C. W. (2006). Connexin 43-mediated modulation of polarized cell movement and the directional migration of cardiac neural crest cells. *Development* **133**, 3629-39.
10. Sohl, G. & Willecke, K. (2003). An update on connexin genes and their nomenclature in mouse and man. *Cell Commun Adhes* **10**, 173-80.

11. Gonzalez-Nieto, D., Gomez-Hernandez, J. M., Larrosa, B., Gutierrez, C., Munoz, M. D., Fasciani, I., O'Brien, J., Zappala, A., Cicirata, F. & Barrio, L. C. (2008). Regulation of neuronal connexin-36 channels by pH. *Proc Natl Acad Sci U S A* **105**, 17169-74.

12. Bargiello, T. A., Tang, Q., Oh, S. & Kwon, T. (2011). Voltage-dependent conformational changes in connexin channels. *Biochim Biophys Acta*.

13. Sohl, G., Odermatt, B., Maxeiner, S., Degen, J. & Willecke, K. (2004). New insights into the expression and function of neural connexins with transgenic mouse mutants. *Brain Res Brain Res Rev* **47**, 245-59.

14. Imbeault, S., Gauvin, L. G., Toeg, H. D., Pettit, A., Sorbara, C. D., Migahed, L., DesRoches, R., Menzies, A. S., Nishii, K., Paul, D. L., Simon, A. M. & Bennett, S. A. (2009). The extracellular matrix controls gap junction protein expression and function in postnatal hippocampal neural progenitor cells. *BMC Neurosci* **10**, 13.

15. Belluardo, N., Mudo, G., Trovato-Salinaro, A., Le Gurun, S., Charollais, A., Serre-Beinier, V., Amato, G., Haefliger, J. A., Meda, P. & Condorelli, D. F. (2000). Expression of connexin36 in the adult and developing rat brain. *Brain Res* **865**, 121-38.

16. Maxeiner, S., Kruger, O., Schilling, K., Traub, O., Urschel, S. & Willecke, K. (2003). Spatiotemporal transcription of connexin45 during brain development results in neuronal expression in adult mice. *Neuroscience* **119**, 689-700.

17. Song, J. H., Wang, Y., Fontes, J. D. & Belousov, A. B. (2012). Regulation of connexin 36 expression during development. *Neurosci Lett* **513**, 17-9.

18. Li, X., Lynn, B. D. & Nagy, J. I. (2012). The effector and scaffolding proteins AF6 and MUPP1 interact with connexin36 and localize at gap junctions that form electrical synapses in rodent brain. *Eur J Neurosci* **35**, 166-81.

19. Hormuzdi, S. G., Pais, I., LeBeau, F. E., Towers, S. K., Rozov, A., Buhl, E. H., Whittington, M. A. & Monyer, H. (2001). Impaired electrical signaling disrupts gamma frequency oscillations in connexin 36-deficient mice. *Neuron* **31**, 487-95.

20. Bedner, P., Niessen, H., Odermatt, B., Kretz, M., Willecke, K. & Harz, H. (2006). Selective permeability of different connexin channels to the second messenger cyclic AMP. *J Biol Chem* **281**, 6673-81.

21. Schock, S. C., Leblanc, D., Hakim, A. M. & Thompson, C. S. (2008). ATP release by way of connexin 36 hemichannels mediates ischemic tolerance in vitro. *Biochem Biophys Res Commun* **368**, 138-44.

22. Pan, F., Paul, D. L., Bloomfield, S. A. & Volgyi, B. (2010). Connexin36 is required for gap junctional coupling of most ganglion cell subtypes in the mouse retina. *J Comp Neurol* **518**, 911-27.

23. Srinivas, M., Rozental, R., Kojima, T., Dermietzel, R., Mehler, M., Condorelli, D. F., Kessler, J. A. & Spray, D. C. (1999). Functional properties of channels formed by the neuronal gap junction protein connexin36. *J Neurosci* **19**, 9848-55.

24. Feigenspan, A., Teubner, B., Willecke, K. & Weiler, R. (2001). Expression of neuronal connexin36 in AII amacrine cells of the mammalian retina. *J Neurosci* **21**, 230-9.

25. Dedek, K., Schultz, K., Pieper, M., Dirks, P., Maxeiner, S., Willecke, K., Weiler, R. & Janssen-Bienhold, U. (2006). Localization of heterotypic gap junctions composed of connexin45 and connexin36 in the rod pathway of the mouse retina. *Eur J Neurosci* **24**, 1675-86.

26. Condorelli, D. F., Belluardo, N., Trovato-Salinaro, A. & Mudo, G. (2000). Expression of Cx36 in mammalian neurons. *Brain Res Brain Res Rev* **32**, 72-85.

27. Gulisano, M., Parenti, R., Spinella, F. & Cicirata, F. (2000). Cx36 is dynamically expressed during early development of mouse brain and nervous system. *Neuroreport* **11**, 3823-8.

28. Hormuzdi, S. G., Filippov, M. A., Mitropoulou, G., Monyer, H. & Bruzzone, R. (2004). Electrical synapses: a dynamic signaling system that shapes the activity of neuronal networks. *Biochim Biophys Acta* **1662**, 113-37.

29. Nagy, J. I. (2012). Evidence for connexin36 localization at hippocampal mossy fiber terminals suggesting mixed chemical/electrical transmission by granule cells. *Brain Res* **1487**, 107-22.

30. Hamzei-Sichani, F., Davidson, K. G., Yasumura, T., Janssen, W. G., Wearne, S. L., Hof, P. R., Traub, R. D., Gutierrez, R., Ottersen, O. P. & Rash, J. E. (2012). Mixed Electrical-Chemical Synapses in Adult Rat Hippocampus are Primarily Glutamatergic and Coupled by Connexin-36. *Front Neuroanat* **6**, 13.

31. Wang, Y., Song, J. H., Denisova, J. V., Park, W. M., Fontes, J. D. & Belousov, A. B. (2012). Neuronal gap junction coupling is regulated by glutamate and plays critical role in cell death during neuronal injury. *J Neurosci* **32**, 713-25.

32. Deans, M. R., Gibson, J. R., Sellitto, C., Connors, B. W. & Paul, D. L. (2001). Synchronous activity of inhibitory networks in neocortex requires electrical synapses containing connexin36. *Neuron* **31**, 477-485.

33. Kistler, W. M., De Jeu, M. T., Elgersma, Y., Van Der Giessen, R. S., Hensbroek, R., Luo, C., Koekkoek, S. K., Hoogenraad, C. C., Hamers, F. P., Gueldenagel, M., Sohl, G., Willecke, K. & De Zeeuw, C. I. (2002). Analysis of Cx36 knockout does not support tenet that olivary gap junctions are required for complex spike synchronization and normal motor performance. *Ann N Y Acad Sci* **978**, 391-404.

34. Long, M. A., Deans, M. R., Paul, D. L. & Connors, B. W. (2002). Rhythmicity without synchrony in the electrically uncoupled inferior olive. *J Neurosci* **22**, 10898-905.

35. Placantonakis, D. G., Bukovsky, A. A., Zeng, X. H., Kiem, H. P. & Welsh, J. P. (2004). Fundamental role of inferior olive connexin 36 in muscle coherence during tremor. *Proc Natl Acad Sci U S A* **101**, 7164-9.

36. Frisch, C., De Souza-Silva, M. A., Sohl, G., Guldenagel, M., Willecke, K., Huston, J. P. & Dere, E. (2005). Stimulus complexity dependent memory impairment and changes in motor performance after deletion of the neuronal gap junction protein connexin36 in mice. *Behav Brain Res* **157**, 177-85.

37. Bissiere, S., Zelikowsky, M., Ponnusamy, R., Jacobs, N. S., Blair, H. T. & Fanselow, M. S. (2011). Electrical synapses control hippocampal contributions to fear learning and memory. *Science* **331**, 87-91.

38. Cruikshank, S. J., Hopperstad, M., Younger, M., Connors, B. W., Spray, D. C. & Srinivas, M. (2004). Potent block of Cx36 and Cx50 gap junction channels by mefloquine. *Proc Natl Acad Sci U S A* **101**, 12364-9.

39. Buhl, D. L., Harris, K. D., Hormuzdi, S. G., Monyer, H. & Buzsaki, G. (2003). Selective impairment of hippocampal gamma oscillations in connexin-36 knock-out mouse in vivo. *J Neurosci* **23**, 1013-8.

40. Wang, Y. & Belousov, A. B. (2011). Deletion of neuronal gap junction protein connexin 36 impairs hippocampal LTP. *Neurosci Lett* **502**, 30-2.

41. Mas, C., Taske, N., Deutsch, S., Guipponi, M., Thomas, P., Covanis, A., Friis, M., Kjeldsen, M. J., Pizzolato, G. P., Villemure, J. G., Buresi, C., Rees, M., Malafosse, A., Gardiner, M., Antonarakis, S. E. & Meda, P. (2004). Association of the connexin36 gene with juvenile myoclonic epilepsy. *J Med Genet* **41**, e93.

42. Dirnagl, U., Iadecola, C. & Moskowitz, M. A. (1999). Pathobiology of ischaemic stroke: an integrated view. *Trends Neurosci* **22**, 391-7.

43. Siushansian, R., Bechberger, J. F., Cechetto, D. F., Hachinski, V. C. & Naus, C. C. (2001). Connexin43 null mutation increases infarct size after stroke. *J Comp Neurol* **440**, 387-94.

44. Decrock, E., Vinken, M., De Vuyst, E., Krysko, D. V., D'Herde, K., Vanhaecke, T., Vandenabeele, P., Rogiers, V. & Leybaert, L. (2009). Connexin-related signaling in cell death: to live or let die? *Cell Death Differ* **16**, 524-36.

45. Decrock, E., De Vuyst, E., Vinken, M., Van Moorhem, M., Vranckx, K., Wang, N., Van Laeken, L., De Bock, M., D'Herde, K., Lai, C. P., Rogiers, V., Evans, W. H., Naus, C. C. & Leybaert, L. (2009). Connexin 43 hemichannels

contribute to the propagation of apoptotic cell death in a rat C6 glioma cell model. *Cell Death Differ* **16**, 151-63.

46. Cusato, K., Bosco, A., Rozental, R., Guimaraes, C. A., Reese, B. E., Linden, R. & Spray, D. C. (2003). Gap junctions mediate bystander cell death in developing retina. *J Neurosci* **23**, 6413-22.

47. Krutovskikh, V. A., Piccoli, C. & Yamasaki, H. (2002). Gap junction intercellular communication propagates cell death in cancerous cells. *Oncogene* **21**, 1989-99.

48. de Rivero Vaccari, J. C., Corriveau, R. A. & Belousov, A. B. (2007). Gap junctions are required for NMDA receptor dependent cell death in developing neurons. *J Neurophysiol* **98**, 2878-86.

49. de Pina-Benabou, M. H., Szostak, V., Kyrozis, A., Rempe, D., Uziel, D., Urban-Maldonado, M., Benabou, S., Spray, D. C., Federoff, H. J., Stanton, P. K. & Rozental, R. (2005). Blockade of gap junctions in vivo provides neuroprotection after perinatal global ischemia. *Stroke* **36**, 2232-7.

50. Frank, D. K., Szymkowiak, B., Josifovska-Chopra, O., Nakashima, T. & Kinnally, K. W. (2005). Single-cell microinjection of cytochrome c can result in gap junction-mediated apoptotic cell death of bystander cells in head and neck cancer. *Head Neck* **27**, 794-800.

51. Wang, Q., Yu, S., Simonyi, A., Sun, G. Y. & Sun, A. Y. (2005). Kainic acid-mediated excitotoxicity as a model for neurodegeneration. *Mol Neurobiol* **31**, 3-16.

52. Engel, J., Jr. (2001). Mesial temporal lobe epilepsy: what have we learned? *Neuroscientist* **7**, 340-52.

53. Jacobson, G. M., Voss, L. J., Melin, S. M., Mason, J. P., Cursons, R. T., Steyn-Ross, D. A., Steyn-Ross, M. L. & Sleigh, J. W. (2010). Connexin36 knockout mice display increased sensitivity to pentylenetetrazol-induced seizure-like behaviors. *Brain Res* **1360**, 198-204.

54. Rogawski, M. A. (2006). Molecular targets versus models for new antiepileptic drug discovery. *Epilepsy Res* **68**, 22-8.

55. Olney, J. W., Rhee, V. & Ho, O. L. (1974). Kainic acid: a powerful neurotoxic analogue of glutamate. *Brain Res* **77**, 507-12.

56. Vincent, P. & Mulle, C. (2009). Kainate receptors in epilepsy and excitotoxicity. *Neuroscience* **158**, 309-23.

57. Malva, J. O., Carvalho, A. P. & Carvalho, C. M. (1998). Kainate receptors in hippocampal CA3 subregion: evidence for a role in regulating neurotransmitter release. *Neurochem Int* **32**, 1-6.

58. Melanson-Drapeau, L. (2006). Connexin-32 Mediated Control of Progenitor Cell Fate in Injured and Uninjured Adult Mouse Brain, University of Ottawa.

59. Scherzer, C. R., Landwehrmeyer, G. B., Kerner, J. A., Counihan, T. J., Kosinski, C. M., Standaert, D. G., Daggett, L. P., Velicelebi, G., Penney, J. B. & Young, A. B. (1998). Expression of N-methyl-D-aspartate receptor subunit mRNAs in the human brain: hippocampus and cortex. *J Comp Neurol* **390**, 75-90.

60. Ben-Ari, Y. & Cossart, R. (2000). Kainate, a double agent that generates seizures: two decades of progress. *Trends Neurosci* **23**, 580-7.

61. Liu, Y., Wong, T. P., Aarts, M., Rooyakkers, A., Liu, L., Lai, T. W., Wu, D. C., Lu, J., Tymianski, M., Craig, A. M. & Wang, Y. T. (2007). NMDA receptor

subunits have differential roles in mediating excitotoxic neuronal death both in vitro and in vivo. *J Neurosci* **27**, 2846-57.

62. Howe, M. L. & Barres, B. A. (2012). A novel role for microglia in minimizing excitotoxicity. *BMC Biol* **10**, 7.

63. Dobrenis, K., Chang, H. Y., Pina-Benabou, M. H., Woodroffe, A., Lee, S. C., Rozental, R., Spray, D. C. & Scemes, E. (2005). Human and mouse microglia express connexin36, and functional gap junctions are formed between rodent microglia and neurons. *J Neurosci Res* **82**, 306-15.

64. Vinet, J., Weering, H. R., Heinrich, A., Kalin, R. E., Wegner, A., Brouwer, N., Heppner, F. L., Rooijen, N., Boddeke, H. W. & Biber, K. (2012). Neuroprotective function for ramified microglia in hippocampal excitotoxicity. *J Neuroinflammation* **9**, 27.

65. Eyo, U. & Dailey, M. E. (2012). Effects of oxygen-glucose deprivation on microglial mobility and viability in developing mouse hippocampal tissues. *Glia* **60**, 1747-60.

66. Ito, D., Imai, Y., Ohsawa, K., Nakajima, K., Fukuuchi, Y. & Kohsaka, S. (1998). Microglia-specific localisation of a novel calcium binding protein, Iba1. *Brain Res Mol Brain Res* **57**, 1-9.

67. Aloisi, F. (2001). Immune function of microglia. *Glia* **36**, 165-79.

68. Turrin, N. P. & Rivest, S. (2006). Tumor necrosis factor alpha but not interleukin 1 beta mediates neuroprotection in response to acute nitric oxide excitotoxicity. *J Neurosci* **26**, 143-51.

69. Gehrmann, J., Matsumoto, Y. & Kreutzberg, G. W. (1995). Microglia: intrinsic immuneffector cell of the brain. *Brain Res Brain Res Rev* **20**, 269-87.

70. Colton, C. A. & Gilbert, D. L. (1987). Production of superoxide anions by a CNS macrophage, the microglia. *FEBS Lett* **223**, 284-8.

71. Banati, R. B., Gehrmann, J., Schubert, P. & Kreutzberg, G. W. (1993). Cytotoxicity of microglia. *Glia* **7**, 111-8.

72. Piani, D., Frei, K., Do, K. Q., Cuenod, M. & Fontana, A. (1991). Murine brain macrophages induced NMDA receptor mediated neurotoxicity in vitro by secreting glutamate. *Neurosci Lett* **133**, 159-62.

73. Thery, C., Chamak, B. & Mallat, M. (1991). Cytotoxic Effect of Brain Macrophages on Developing. *Eur J Neurosci* **3**, 1155-1164.

74. Eichhoff, G., Brawek, B. & Garaschuk, O. (2011). Microglial calcium signal acts as a rapid sensor of single neuron damage in vivo. *Biochim Biophys Acta* **1813**, 1014-24.

75. Hoffmann, A., Kann, O., Ohlemeyer, C., Hanisch, U. K. & Kettenmann, H. (2003). Elevation of basal intracellular calcium as a central element in the activation of brain macrophages (microglia): suppression of receptor-evoked calcium signaling and control of release function. *J Neurosci* **23**, 4410-9.

76. Lalancette-Hebert, M., Gowing, G., Simard, A., Weng, Y. C. & Kriz, J. (2007). Selective ablation of proliferating microglial cells exacerbates ischemic injury in the brain. *J Neurosci* **27**, 2596-605.

77. El Khoury, J., Toft, M., Hickman, S. E., Means, T. K., Terada, K., Geula, C. & Luster, A. D. (2007). Ccr2 deficiency impairs microglial accumulation and accelerates progression of Alzheimer-like disease. *Nat Med* **13**, 432-8.

78. van Rossum, D. & Hanisch, U. K. (2004). Microglia. *Metab Brain Dis* **19**, 393-411.

79. Condorelli, D. F., Trovato-Salinaro, A., Mudo, G., Mirone, M. B. & Belluardo, N. (2003). Cellular expression of connexins in the rat brain: neuronal localization, effects of kainate-induced seizures and expression in apoptotic neuronal cells. *Eur J Neurosci* **18**, 1807-27.

80. Sohl, G., Guldenagel, M., Beck, H., Teubner, B., Traub, O., Gutierrez, R., Heinemann, U. & Willecke, K. (2000). Expression of connexin genes in hippocampus of kainate-treated and kindled rats under conditions of experimental epilepsy. *Brain Res Mol Brain Res* **83**, 44-51.

81. Connors, B. W. & Long, M. A. (2004). Electrical synapses in the mammalian brain. *Annu Rev Neurosci* **27**, 393-418.

82. Deans, M. R., Gibson, J. R., Sellitto, C., Connors, B. W. & Paul, D. L. (2001). Synchronous activity of inhibitory networks in neocortex requires electrical synapses containing connexin36. *Neuron* **31**, 477-85.

83. Bennett, S. A., Stevenson, B., Staines, W. A. & Roberts, D. C. (1995). Periodic acid-Schiff (PAS)-positive deposits in brain following kainic acid-induced seizures: relationships to fos induction, neuronal necrosis, reactive gliosis, and blood-brain barrier breakdown. *Acta Neuropathol* **89**, 126-38.

84. Jensen, A. M. & Wallace, V. A. (1997). Expression of Sonic hedgehog and its putative role as a precursor cell mitogen in the developing mouse retina. *Development* **124**, 363-71.

85. Schneider, C. A., Rasband, W. S. & Eliceiri, K. W. (2012). NIH Image to ImageJ: 25 years of image analysis. *Nat Methods* **9**, 671-5.

86. Pettit, A. S., Desroches, R. & Bennett, S. A. (2012). The opiate analgesic buprenorphine decreases proliferation of adult hippocampal neuroblasts and increases survival of their progeny. *Neuroscience* **200**, 211-22.

87. Thallmair, M., Ray, J., Stallcup, W. B. & Gage, F. H. (2006). Functional and morphological effects of NG2 proteoglycan deletion on hippocampal neurogenesis. *Exp Neurol* **202**, 167-78.

88. Guo, F., Maeda, Y., Ma, J., Xu, J., Horiuchi, M., Miers, L., Vaccarino, F. & Pleasure, D. (2010). Pyramidal neurons are generated from oligodendroglial progenitor cells in adult piriform cortex. *J Neurosci* **30**, 12036-49.

89. Ross, F. M., Gwyn, P., Spanswick, D. & Davies, S. N. (2000). Carbenoxolone depresses spontaneous epileptiform activity in the CA1 region of rat hippocampal slices. *Neuroscience* **100**, 789-96.

90. Pickering, A. E., Spanswick, D. & Logan, S. D. (1991). Whole-cell recordings from sympathetic preganglionic neurons in rat spinal cord slices. *Neurosci Lett* **130**, 237-42.

91. Cheung, E. C., Melanson-Drapeau, L., Cregan, S. P., Vanderluit, J. L., Ferguson, K. L., McIntosh, W. C., Park, D. S., Bennett, S. A. L. & Slack, R. S. (2005). Apoptosis-inducing factor is a key factor in neuronal cell death propagated by BAX-dependent and BAX-independent mechanisms. *J Neurosci* **25**, 1324-34.

92. Cheung, E. C., Melanson-Drapeau, L., Cregan, S. P., Vanderluit, J. L., Ferguson, K. L., McIntosh, W. C., Park, D. S., Bennett, S. A. & Slack, R. S. (2005). Apoptosis-inducing factor is a key factor in neuronal cell death

propagated by BAX-dependent and BAX-independent mechanisms. *J Neurosci* **25**, 1324-34.

93. Pais, I., Hormuzdi, S. G., Monyer, H., Traub, R. D., Wood, I. C., Buhl, E. H., Whittington, M. A. & LeBeau, F. E. (2003). Sharp wave-like activity in the hippocampus in vitro in mice lacking the gap junction protein connexin 36. *J Neurophysiol* **89**, 2046-54.

94. Unal-Cevik, I., Kilinc, M., Gursoy-Ozdemir, Y., Gurer, G. & Dalkara, T. (2004). Loss of NeuN immunoreactivity after cerebral ischemia does not indicate neuronal cell loss: a cautionary note. *Brain Res* **1015**, 169-74.

95. Sharma, A. K., Reams, R. Y., Jordan, W. H., Miller, M. A., Thacker, H. L. & Snyder, P. W. (2007). Mesial temporal lobe epilepsy: pathogenesis, induced rodent models and lesions. *Toxicol Pathol* **35**, 984-99.

96. Aimone, J. B., Wiles, J. & Gage, F. H. (2006). Potential role for adult neurogenesis in the encoding of time in new memories. *Nat Neurosci* **9**, 723-7.

97. Bargiotas, P., Muhammad, S., Rahman, M., Jakob, N., Trabold, R., Fuchs, E., Schilling, L., Plesnila, N., Monyer, H. & Schwaninger, M. (2012). Connexin 36 promotes cortical spreading depolarization and ischemic brain damage. *Brain Res* **1479**, 80-5.

98. Ma, Y., Hioki, H., Konno, M., Pan, S., Nakamura, H., Nakamura, K. C., Furuta, T., Li, J. L. & Kaneko, T. (2011). Expression of gap junction protein connexin36 in multiple subtypes of GABAergic neurons in adult rat somatosensory cortex. *Cereb Cortex* **21**, 2639-49.

99. Mills, S. L., O'Brien, J. J., Li, W., O'Brien, J. & Massey, S. C. (2001). Rod pathways in the mammalian retina use connexin 36. *J Comp Neurol* **436**, 336-50.

100. Shetty, A. K., Hattiangady, B. & Rao, M. S. (2009). Vulnerability of hippocampal GABA-ergic interneurons to kainate-induced excitotoxic injury during old age. *J Cell Mol Med* **13**, 2408-23.

101. Dong, H., Csernansky, C. A., Goico, B. & Csernansky, J. G. (2003). Hippocampal neurogenesis follows kainic acid-induced apoptosis in neonatal rats. *J Neurosci* **23**, 1742-9.

102. Mulle, C., Sailer, A., Perez-Otano, I., Dickinson-Anson, H., Castillo, P. E., Bureau, I., Maron, C., Gage, F. H., Mann, J. R., Bettler, B. & Heinemann, S. F. (1998). Altered synaptic physiology and reduced susceptibility to kainate-induced seizures in GluR6-deficient mice. *Nature* **392**, 601-5.

103. Liang, K. C., Hon, W., Tyan, Y. M. & Liao, W. L. (1994). Involvement of hippocampal NMDA and AMPA receptors in acquisition, formation and retrieval of spatial memory in the Morris water maze. *Chin J Physiol* **37**, 201-12.

104. Lima, P. A., Nardi, G. & Brown, E. R. (2003). AMPA/kainate and NMDA-like glutamate receptors at the chromatophore neuromuscular junction of the squid: role in synaptic transmission and skin patterning. *Eur J Neurosci* **17**, 507-16.

105. Lee, J. Y., Bhatt, D., Bhatt, D., Chung, W. Y. & Cooper, R. L. (2009). Furthering pharmacological and physiological assessment of the

glutamatergic receptors at the Drosophila neuromuscular junction. *Comp Biochem Physiol C Toxicol Pharmacol* **150**, 546-57.

106. Shetty, A. K. (2011). Progress in cell grafting therapy for temporal lobe epilepsy. *Neurotherapeutics* **8**, 721-35.

107. Vonck, K., De Herdt, V. & Boon, P. (2009). Vagal nerve stimulation--a 15-year survey of an established treatment modality in epilepsy surgery. *Adv Tech Stand Neurosurg* **34**, 111-46.

108. Ochoa, J. (1994). Antiepileptic Drugs (Benbadis, S., ed.), Vol. 2013. WebMD LLC, Medscape Reference.

109. Luszczki, J. J. (2009). Third-generation antiepileptic drugs: mechanisms of action, pharmacokinetics and interactions. *Pharmacol Rep* **61**, 197-216.

110. Rodriguez-Sainz, A., Pinedo-Brochado, A., Sanchez-Menoyo, J. L., Ruiz-Ojeda, J., Escalza-Cortina, I. & Garcia-Monco, J. C. (2013). Migraine, Stroke and Epilepsy: Underlying and Interrelated Causes, Diagnosis and Treatment. *Curr Treat Options Cardiovasc Med*.

111. Devinsky, O. (2004). Therapy for neurobehavioral disorders in epilepsy. *Epilepsia* **45 Suppl 2**, 34-40.

112. Trojnar, M. K., Malek, R., Chroscinska, M., Nowak, S., Blaszczyk, B. & Czuczwar, S. J. (2002). Neuroprotective effects of antiepileptic drugs. *Pol J Pharmacol* **54**, 557-66.

113. Pitkanen, A. & Kubova, H. (2004). Antiepileptic drugs in neuroprotection. *Expert Opin Pharmacother* **5**, 777-98.

114. Fattore, C. & Perucca, E. (2011). Novel medications for epilepsy. *Drugs* **71**, 2151-78.

Statement of contributions

Electrophysiology studies were performed in collaboration with Dr. David Spanswick. My role was to prepare the animals, assist in the acute slice preparation, observe the electrophysiology, assist in the analysis of the data, and interpret the results. NeuN+, H&E, and TUNEL+ counts and figures in KA-injury time course models were completed in collaboration with a M.Sc. student in the Bennett laboratory Catherine Sorbara. I performed KA-injury, NeuN immuno-labeling, counted cells, and interpreted results. Western blot analysis of Cx36 expression in a time course post KA-injury was performed in collaboration with a post-doctoral fellow in the Bennett laboratory Dr. Leigh-Anne Swayne. I performed the KA-injury, brain dissection, assisted with the western blotting, and interpreted the results. I would like to acknowledge Crystal Hanley, who was part of the CIHR Training Program in Neurodegenerative Lipidomics, for creating the adhesion domains portion of Figure 1 (Fig. 1 i). I would like to acknowledge Matthew Lenardis and Bettina Franko for assisting me, running portions of MWM behaviour trials. I performed all other experiments in this thesis without additional assistance.